Behavioral/Systems/Cognitive

Spontaneous High-Frequency (10–80 Hz) Oscillations during Up States in the Cerebral Cortex *In Vitro*

Albert Compte,[1,2] Ramon Reig,[1,2] Vanessa F. Descalzo,[1,2] Michael A. Harvey,[2] Gabriel D. Puccini,[2] and Maria V. Sanchez-Vives[1,2,3]

[1]Institut d'Investigacions Biomèdiques August Pi i Sunyer (IDIBAPS), 08036 Barcelona, Spain, [2]Instituto de Neurociencias de Alicante, Universidad Miguel Hernández-Consejo Superior de Investigaciones Científicas, 03550 Sant Joan d'Alacant, Spain, and [3]Institució Catalana de Recerca i Estudis Avançats (ICREA), 08010 Barcelona, Spain

High-frequency oscillations in cortical networks have been linked to a variety of cognitive and perceptual processes. They have also been recorded in small cortical slices *in vitro*, indicating that neuronal synchronization at these frequencies is generated in the local cortical circuit. However, *in vitro* experiments have hitherto necessitated exogenous pharmacological or electrical stimulation to generate robust synchronized activity in the β/γ range. Here, we demonstrate that the isolated cortical microcircuitry generates β and γ oscillations spontaneously in the absence of externally applied neuromodulators or synaptic agonists. We show this in a spontaneously active slice preparation that engages in slow oscillatory activity similar to activity during slow-wave sleep. β and γ synchronization appeared during the up states of the slow oscillation. Simultaneous intracellular and extracellular recordings revealed synchronization between the timing of incoming synaptic events and population activity. This rhythm was mechanistically similar to pharmacologically induced γ rhythms, as it also included sparse, irregular firing of neurons within the population oscillation, predominant involvement of inhibitory neurons, and a decrease of oscillation frequency after barbiturate application. Finally, we show in a computer model how a synaptic loop between excitatory and inhibitory neurons can explain the emergence of both the slow (<1 Hz) and the β-range oscillations in the neocortical network. We therefore conclude that oscillations in the β/γ range that share mechanisms with activity reported *in vivo* or in pharmacologically activated *in vitro* preparations can be generated during slow oscillatory activity in the local cortical circuit, even without exogenous pharmacological or electrical stimulation.

Key words: **γ; β; microcircuit; synchronization; inhibition; slow oscillations**

Introduction

In the local cortical circuit, enhanced synchronization of neural activity at frequencies in the β and γ ranges (10–100 Hz) has been linked to cognitive operations such as selective attention (Steinmetz et al., 2000; Fries et al., 2001; Womelsdorf et al., 2006; Saalmann et al., 2007) or working memory (Tallon-Baudry et al., 1998; Pesaran et al., 2002; Tallon-Baudry et al., 2004), as well as the formation of sensory percepts (Singer and Gray, 1995; Fries et al., 1997; Fries et al., 2002; Gross et al., 2007). Long-range synchronization between cortical local circuits at different levels of hierarchical processing is thought to underlie this functional synchronization enhancement (Melloni et al., 2007; Saalmann et al., 2007; Womelsdorf et al., 2007), but the generation of synchronous neural activity may largely rely on the physiological machinery of the local cortical circuitry. Evidence for this comes from *in vitro* recordings in acute brain slices, which have shown that isolated local cortical circuits are capable of generating oscillatory population activity in the β and γ range (Whittington et al., 1995, 1997; Buhl et al., 1998; Fisahn et al., 1998; Fellous and Sejnowski, 2000; LeBeau et al., 2002; Cunningham et al., 2003; Hasenstaub et al., 2005; Traub et al., 2005; Bibbig et al., 2007). These experiments have usually relied on pharmacological activation, typically with carbachol (CCh) or kainate, or electrical tetanic stimulation of the tissue, in conditions that did not replicate specific physiological network states *in vivo* (Traub et al., 2004). Together, this could suggest that β/γ-range oscillatory activity does not emerge spontaneously in the isolated cortical circuit, and is dependent on specific neuromodulators for its generation (Börgers et al., 2005).

Interestingly, Steriade et al. (1996) found that γ oscillations occurred during the activated phases of the slow oscillations (<1 Hz) in anesthetized cats. This physiological network state characterizes slow-wave sleep (Steriade et al., 1993) and it can be reproduced approximately *in vitro* (Sanchez-Vives and McCormick, 2000). Here, we scrutinize slow oscillations *in vitro* to test whether fast oscillatory activity can emerge from the isolated cortical network in the absence of additional pharmacological or electrical stimulation. We analyze the activity from slices of ferret

Received May 29, 2008; revised Nov. 3, 2008; accepted Nov. 8, 2008.

This work was supported by the Spanish Ministry of Science and Innovation and the European Regional Development Fund. A.C. was supported by a Ramón y Cajal Research Fellowship of the Spanish Ministry of Science and is currently supported by the Researcher Stabilization Program of the Health Department of the Generalitat de Catalunya.

Correspondence should be addressed to Albert Compte or Maria V. Sanchez-Vives, Institut d'Investigacions Biomèdiques August Pi i Sunyer (IDIBAPS), Villarroel 170, 08036 Barcelona, Spain. E-mail: acompte@clinic.ub.es or msanche3@clinic.ub.es.

DOI:10.1523/JNEUROSCI.2684-08.2008

 0270-6474/08/2813828-17$15.00/0

cerebral cortex during slow oscillatory activity and apply multitaper spectral methods to study the temporal properties of network activity during activated states. Through simultaneous intracellular and local field potential recordings, we assess the differential implication of excitatory and inhibitory neurons in these rhythms. Finally, we evaluate specific mechanistic predictions, based on a detailed biophysical computer model of combined slow and β/γ rhythm generation (Compte et al., 2003a). Although we also see that neuromodulators potently modulate β/γ-range activity, robust β/γ-range activity emerges already during physiological network function in the absence of externally applied neuromodulatory agents and without any particular stimulation pattern. Neuromodulators are therefore modifying the properties of an intrinsic β/γ rhythm of the local cortical circuit, rather than modifying the network physiology so it can sustain β/γ-range oscillations.

Materials and Methods

In vitro *experiments*

Slice preparation. The methods for preparing cortical slices were similar to those described previously (Reig and Sanchez-Vives, 2007). Briefly, cortical slices were prepared from 3- to 8-month-old ferrets of either sex that were deeply anesthetized with sodium pentobarbital (40 mg/kg) and decapitated. Four hundred-micrometer-thick coronal slices of the visual or prefrontal cortex were cut on a Vibratome. A modification of the technique developed by (Aghajanian and Rasmussen, 1989) was used to increase tissue viability. After preparation, slices were placed in an interface-style recording chamber (Fine Sciences Tools) and bathed in ACSF containing (in mM): NaCl, 124; KCl, 2.5; $MgSO_4$, 2; $NaHPO_4$, 1.25; $CaCl_2$, 2; $NaHCO_3$, 26; and dextrose, 10, and was aerated with 95% O_2, 5% CO_2 to a final pH of 7.4. Bath temperature was maintained at 35–36°C. Recordings were initiated after 2 h of recovery. In order for spontaneous rhythmic activity to be generated, the solution was switched to "*in vivo*-like" ACSF containing (in mM): NaCl, 124; KCl, 3.5; $MgSO_4$, 1; $NaHPO_4$, 1.25; $CaCl_2$, 1.2; $NaHCO_3$, 26; and dextrose, 10 (Sanchez-Vives and McCormick, 2000).

Recordings and stimulation. Extracellular multiunit recordings were obtained from different cortical layers with 2–4 MΩ tungsten electrodes (FHC) and amplified using a Neurolog system (Digitimer). The signal was recorded unfiltered at a sampling frequency between 1 and 10 kHz. For intracellular recordings (sampling frequency 5–10 kHz), sharp electrodes were formed on a Sutter Instruments P-97 micropipette puller from medium-walled glass and beveled to final resistances of 50–100 MΩ. Micropipettes were filled with 2 M potassium acetate. In the experiments in which synaptic activity during oscillations was evaluated, both intra and extracellular recordings were obtained from very close locations (<100 μm) always within the same cortical layer. Sodium channel blocker QX314 (100 μM) was often included in the electrode solution to better hold the membrane voltage (V_m) at depolarized potentials while preventing firing. A pneumatic picopump (WPI) was used to deliver pressure for 10–100 ms at the back of a broken pipette (1–4 μm tip diameter) to extrude 1–20 pl of solution. Both thiopental (Braun Medical) and carbachol (Sigma) were either applied locally by these means, or to the whole network by adding the drug to the ACSF entering the recording chamber. Recordings were digitized and acquired totally unfiltered using a data acquisition interface and software from Cambridge Electronic Design.

Analysis

Extracellular signals. Three types of signals were extracted from the unfiltered extracellular recordings. Local field potential (LFP) was the signal obtained by bandpass filtering the extracellular recording between 2 and 150 Hz. The multiunit extracellular signal (MU) was obtained by high-pass filtering the extracellular recording at 5 Hz, so it also contained the high-frequency components associated with spiking activity. The multiunit spiking activity (MUA) was obtained by high-pass filtering the extracellular recording at 250 Hz and thresholding it to obtain the times of the fastest events, likely reflecting action potentials recorded extracellularly.

Extraction of up state-down state transitions. Local field potentials (see Fig. 1*A*, see solid trace) were used to identify up state and down state onsets. The envelope of the local field potential was evaluated as the amplitude of its analytic signal (complex Hilbert transform), high-pass filtered 0.1 Hz to remove the DC, and smoothed with a running-average square window of 100 ms (see Fig. 1*A*, dashed trace). The mean value of this signal was the threshold for the detection of transitions between up state and down state in all recordings (see Fig. 1*A*, dotted line). To have long enough time series for subsequent analyses, detected up states or down states shorter than 400 ms were discarded from the final list of detected transitions (see Fig. 1*A*, solid dark bars indicate up states).

Detection of intracellular synaptic events. The timing of synaptic events was detected from sharp voltage deflections in intracellular recordings. These were identified by applying a Parks-McClellan low-pass differentiator filter (order 20, cutoff at 200 Hz) and selecting local maxima (for EPSPs) or minima (for IPSPs) beyond a threshold value determined with a statistical criterium (see Fig. 5*E*). Inhibitory events were more reliably detected at depolarized holding voltages (~0 mV), whereas excitatory events were most clear at holding voltages near the reversal potential of $GABA_A$ receptors (−70 mV). The method is presented in the Results section and in Figure 5. This analysis may present certain limitations. Highly synchronous events may be underestimated by being considered under the same detected event. Because of the higher synchronization of inhibitory neurons (see Discussion), this may affect especially inhibitory events. Slower postsynaptic voltage dynamics will also prevent detection. Different excitatory and inhibitory potential kinetics could thus bias the detection toward faster, sharper events. Finally, our derivative method used a low-pass filter with cutoff at 200 Hz. This will also limit the detection of closely spaced events (< 5 ms). Because we are interested in rhythms significantly slower than these limitations, and the caveats apply equally to excitation and inhibition, the method is still a valuable tool for our analyses. We address these caveats by confirming our results with other independent signals (membrane voltage and MUA, see Figs. 7, 8, 9) and by looking at their distribution across different membrane potentials (see Fig. 5*E*). The agreement with results using these other signals supports the validity of the method.

Spectral analysis. Multitaper spectral estimates were used to compute power spectra and cross-spectra, both of time series and point processes (Percival and Walden, 1993). These methods allow for the control of the bias and variance of the spectral estimate (Percival and Walden, 1993), and their usage for electrophysiological signals is well documented (Mitra and Pesaran, 1999; Jarvis and Mitra, 2001).

Time series data (extracellular and intracellular signals) were collected as segments of data of prescribed length T (of the length of up state duration, typically 0.4–1 s) from the time of detected transitions (down state-to-up state or up state-to-down state, as required by the analysis). The data thus consisted of as many data segments as detected transitions N, and these pieces of data were treated as reflecting independent realizations of the network dynamics. We computed Fourier transforms $S(f)$ on our data segments windowed by the first n tapers of the Slepian sequences (Percival and Walden, 1993). The number of tapers used n was dependent on the temporal length T of the segment, such that the transform had a bandwidth of $W \approx 2$ Hz ($n \simeq 2TW - 1$). At this point, the data were represented in frequency-domain by $N \times n$ Fourier transforms $S_{ij}(f)$. From these quantities we could compute the power spectrum as the average squared magnitude of the transforms:

$$I(f) = \frac{1}{Nn}\sum_{i=1}^{N}\sum_{j=1}^{n}|S_{ij}(f)|^2, \quad (1)$$

and the cross-spectrum between two sets A and B of data recorded simultaneously (for instance, extracellular and intracellular data) was computed as:

$$I_{AB}(f) = \frac{1}{Nn}\sum_{i=1}^{N}\sum_{j=1}^{n}S_{ij}^{A}(f)S_{ij}^{B}(f)^{\star} \quad (2)$$

(star superscript denoting complex-conjugation). The complex-valued coherency of the data sets A and B is calculated from the cross-spectrum and the corresponding power spectra:

$$C_{AB}(f) = I_{AB}(f) \Big/ \sqrt{I_{AA}(f) I_{BB}(f)}. \quad (3)$$

The coherence between the sets of data A and B is the squared magnitude of the coherency $|C_{AB}(f)|^2$. This coherence estimate is tested against the null hypothesis that sets A and B are independent. Under this hypothesis, the coherence is zero at all frequencies and the upper 95% confidence interval (CI) is given by $1 - (0.05)^{1/(N \times n - 1)}$ (Halliday et al., 1995). The inverse Fourier transform of the power spectrum (Eq. 1) and the cross-spectrum (Eq. 2) yield the autocorrelation function and the cross-correlation function, respectively. The variance of these spectral quantities was calculated using a jackknife method (Thomson and Chave, 1991).

From our point process data (excitatory/inhibitory synaptic events, see Fig. 5, and multiunit events), we extracted segments of fixed length T (of the length of up state duration, typically 0.4–1 s) at each detected down state-to-up state transition (see above). For each of these N event-train segments, a continuous process was built by replacing each event by a δ function and subtracting the average rate, then each segment was sequentially windowed with the first n tapers of the Slepian sequences (analogous to time series data above), and we subsequently processed these data with Fourier transforms to obtain $S_{ij}(f)$, and from there the spectral estimates described by Equations 1 and 2. Thus, the event-field coherence was obtained from Equation 3, taking $S^A_{ij}(f)$ from the extracellular data segments and $S^B_{ij}(f)$ from the relevant event train data (Halliday et al., 1995). In addition, the event-field-event coherency was computed as $C_{AB}(f)C_{AC}(f)^\star$, with the data set A being the extracellular signal, and the data sets B and C the excitatory and inhibitory synaptic events, respectively, obtained from the intracellular record at different holding potentials (see Fig. 3).

Although the short duration of the data segments facilitated a stationarity assumption, our methods can also be applied to nonstationary signals, but the interpretation of the results is more difficult, especially at low frequencies. The 95% CIs were computed as 1.96 times the SD of the normalized spectra, which was calculated using a jackknife method over trials (Thomson and Chave, 1991). This method provides a robust estimator of the variance of the spectrum, even in the presence of nonstationarities. Our analysis did not address frequencies <5 Hz given the length T of the time-window.

To obtain population quantities, we averaged power spectra, coherency and coherence across neurons in our database. The variance of this average was calculated using a jackknife method over neurons, and from it, 95% CIs were computed as 1.96 times the SD.

All analysis was performed in Matlab (MathWorks).

Computational modeling

We used the network model of (Compte et al., 2003a), with exactly the same parameters as in their control condition. Briefly, the network model consists of a population of 1024 pyramidal cells and 256 interneurons equidistantly distributed on a line and interconnected through biologically plausible synaptic dynamics. Some of the intrinsic parameters of the cells are randomly distributed, so that the populations are heterogeneous. This and the random connectivity are the only sources of noise in the network.

Our model pyramidal cells have a somatic and a dendritic compartment. The spiking currents, I_{Na} and I_K, are located in the soma, together with a leak current I_L, a fast A-type K^+-current I_A, a non-inactivating slow K^+-current I_{KS} and a Na^+-dependent K^+-current I_{KNa}. The dendrite contains a high-threshold Ca^{2+} current I_{Ca}, a Ca^{2+}-dependent K^+-current I_{KCa}, a noninactivating (persistent) Na^+ current I_{NaP} and an inward rectifier (activated by hyperpolarization) noninactivating K^+ current I_{AR}. Explicit equations and parameters for these Hodgkin-Huxley-type currents can be found in (Compte et al., 2003a). In our simulations, all excitatory synapses target the dendritic compartment and all inhibitory synapses are localized on the somatic compartment of postsynaptic pyramidal neurons. Interneurons are modeled with just Hodgkin-Huxley spiking currents, I_{Na} and I_K, and a leak current I_L in their single compartment (Wang and Buzsáki, 1996). Model pyramidal neurons set according to these parameters fire at an average of 22 Hz when they are injected a depolarizing current of 0.25 nA for 0.5 s. The firing pattern corresponds to a regular spiking neuron with some adaptation. In contrast, a model interneuron fires at ~75 Hz when equally stimulated and has the firing pattern of a fast spiking neuron.

Synaptic currents are conductance-based and their kinetics are modeled to mimic AMPAR-, NMDAR-, and $GABA_A$R-mediated synaptic transmission (Wang, 1999; Compte et al., 2003a). All parameters for synaptic transmission are taken from the control network in (Compte et al., 2003a). These values were chosen so that the network would show stable periodic propagating discharges with characteristics compatible with experimental observations. No specific tuning was done taking into account fast-frequency oscillations, which are the object of study here.

The neurons in the network are sparsely connected to each other through a fixed number of connections that are set at the beginning of the simulation. Neurons make 20 ± 5 contacts (mean ± SD) to their postsynaptic partners (multiple contacts onto the same target, but no autapses, are allowed). For each pair of neurons, the probability that they are connected in each direction is decided by a Gaussian probability distribution centered at 0 and with a prescribed SD (Compte et al., 2003a).

The model was implemented in a C++ code and simulated using a forth-order Runge–Kutta method with a time-step of 0.06 ms.

Results

Simultaneous extracellular and intracellular recordings were obtained from 65 spontaneously active slices of ferret visual (n = 54) and prefrontal (n = 11) cortex. These slices became spontaneously active when bathed in an ionic solution that is known to lead to a slow (< 1 Hz) oscillatory rhythm (Sanchez-Vives and McCormick, 2000), reminiscent of physiological activity during slow wave sleep (Steriade et al., 1993). At the single cell level, this type of activity is characterized by the recurring transition of the membrane voltage between a depolarized state coronated with action potentials (up state) and a hyperpolarized state (down state). Because neighboring neurons undergo these transitions coherently (Crochet et al., 2005; Volgushev et al., 2006), this is also reflected in extracellular recordings as an amplification of the fluctuations in the LFP signal (obtained by bandpass filtering the extracellular recording between 2 and 150 Hz) (Mukovski et al., 2007). We analyzed both sharp-electrode intracellular recordings and extracellular signals recorded in close proximity to relate activity observed at the single cell level with the embedded network dynamics. Thus, a preliminary analysis common to all our further explorations was the extraction from the extracellular signals of the times of transition between up states and down states. Such information was later used to select pieces of the intracellular or extracellular record according to the period selected to be analyzed: up state, down state, beginning of up state, or end of up state. The algorithm used to extract the times of transition between up and down states is explained in detail in Materials and Methods, and illustrated graphically in Figure 1*A*. In brief, an envelope of the LFP was calculated and it was thresholded at its mean value to determine the times at which the population coherently underwent one of these transitions. If the signal stayed above (below) this threshold for at least 400 ms we defined the period until a subsequent below-threshold (above-threshold) transition as an up state (down state). Figure 1*B* shows pieces of the LFP aligned at detected down state-to-up state transitions, showing that this analysis indeed produced an accurate detection of these transitions. Up states detected from the LFP in this way had a mean duration of 752 ± 28 ms (mean ± SEM; range 436–1671 ms) and down states lasted for an average 2.3 ± 0.15 s (mean ± SEM; range 0.6–6.4 ms). Down states were sig-

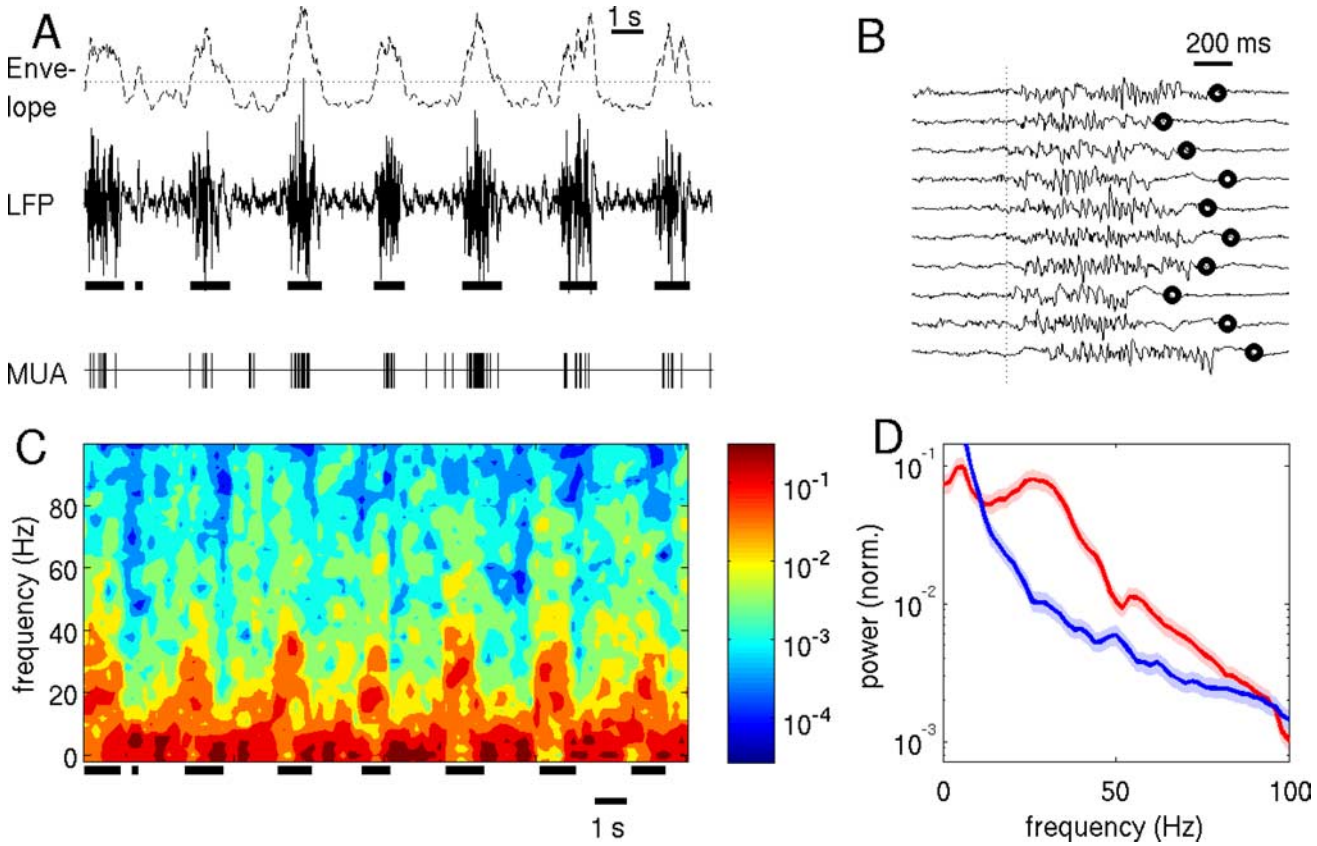

Figure 1. The spontaneously active cortical slice showed high-frequency activity during the up state of the slow oscillation. ***A***, The envelope of the recorded LFP was extracted and thresholded (top trace) from the raw signal (middle trace, sampling frequency 2 kHz) to obtain the onset and offset times of up states of the slow oscillation (indicated with black bars). Alternatively, multiunit activity (bottom trace) was obtained by high-pass filtering the signal and thresholding it. ***B***, This procedure was automatized and routinely checked by plotting fragments of the raw LFP aligned to the identified up state onset times (dotted vertical line). Up state offset times are indicated with a circle on each trace. ***C***, Example of spectrogram (multitaper power spectrum estimates normalized to variance, see Materials and Methods, on sliding windows of 0.5 s, stepped by 0.25 s) showing the co-occurrence of up states (black bars along *x*-axis) and spectral amplification at high frequencies. ***D***, Same data as in ***C*** but now estimating the power spectrum independently for up states (in red, fragments of 0.5-s duration from up state onset time) and down states (in blue, fragments of 0.5-s duration from up state offset time). Shades indicate 95% CIs showing a significant increase of power between 10 and 80 Hz during up states.

nificantly longer than up states (one-tailed paired t test, $p < 0.001$, $n = 81$). Note that especially the length of up states is overestimated because we discarded states shorter than 400 ms to have sufficient data for our spectral methods.

Fast network oscillations during up states

We first analyzed the spectral content of the LFP separating up state and down state periods of the network spontaneous activity. We wanted to address the question of whether this coherent activation of the cortical network (up state) had a specific spectral fingerprint. Absolute spectral power values are of little practical interest here, as by the very selection of up states and down states we anticipate up state signals to have more power than down states. Indeed, the time integral of the power spectrum of a time series is the variance of the time series, and our up state-down state detector is based on the selection of high-variance periods as up states (Fig. 1*A*,*B*). If the only difference between up states and down states was an overall increase of neural activity without any specific temporal rearrangement of events, LFP signals at either period would be statistically indistinguishable except for a scaling factor. This would translate in power spectra of up state and down states being scaled versions of each other. We tested this hypothesis by plotting the power spectra at either period normalized by the variance of the signal. Multitaper power spectra were computed as detailed in Materials and Methods, and allowed for the evaluation of 95% CIs on these spectral estimates. We found that in most of our recordings the normalized spectrum of LFPs during up states differed significantly from the normalized spectrum during down states in the β and lower γ range (β/γ band) (Fig. 1*C*,*D*). Indeed, significantly enhanced power in the range 5–30 Hz was observed in 46 of 65 recorded slices. This corresponded to 40/54 slices of the visual cortex and 6/11 slices of the prefrontal cortex. These proportions were not significantly different using a z test, $z = 1.21$ $p > 0.05$, and we pooled data from these two data sets for our subsequent analyses. We also pooled together data from the various cortical layers since we could not identify a significant association between layer and the enhanced frequency band in up states (Fisher's exact test $p = 0.14$, $n = 86$). This is in contrast with recent data, showing a laminar specificity of high-frequency activity (Roopun et al., 2006). However, our data cannot address this issue rigorously as we did not obtain simultaneous recordings in different layers.

Thus, the activity recorded from cortical slices revealed that up states were characterized not only by an overall enhancement of fluctuations in the signal, but also by a relative increase of spectral power in the β/γ band. This suggests that during the periods of reverberant cortical network activation neural activity organizes temporally and acquires an oscillatory character at β and low γ frequencies. This finding parallels results obtained *in vivo* (Mukovski et al., 2007), but there the range of frequencies for which the spectral power is boosted during up states is broader

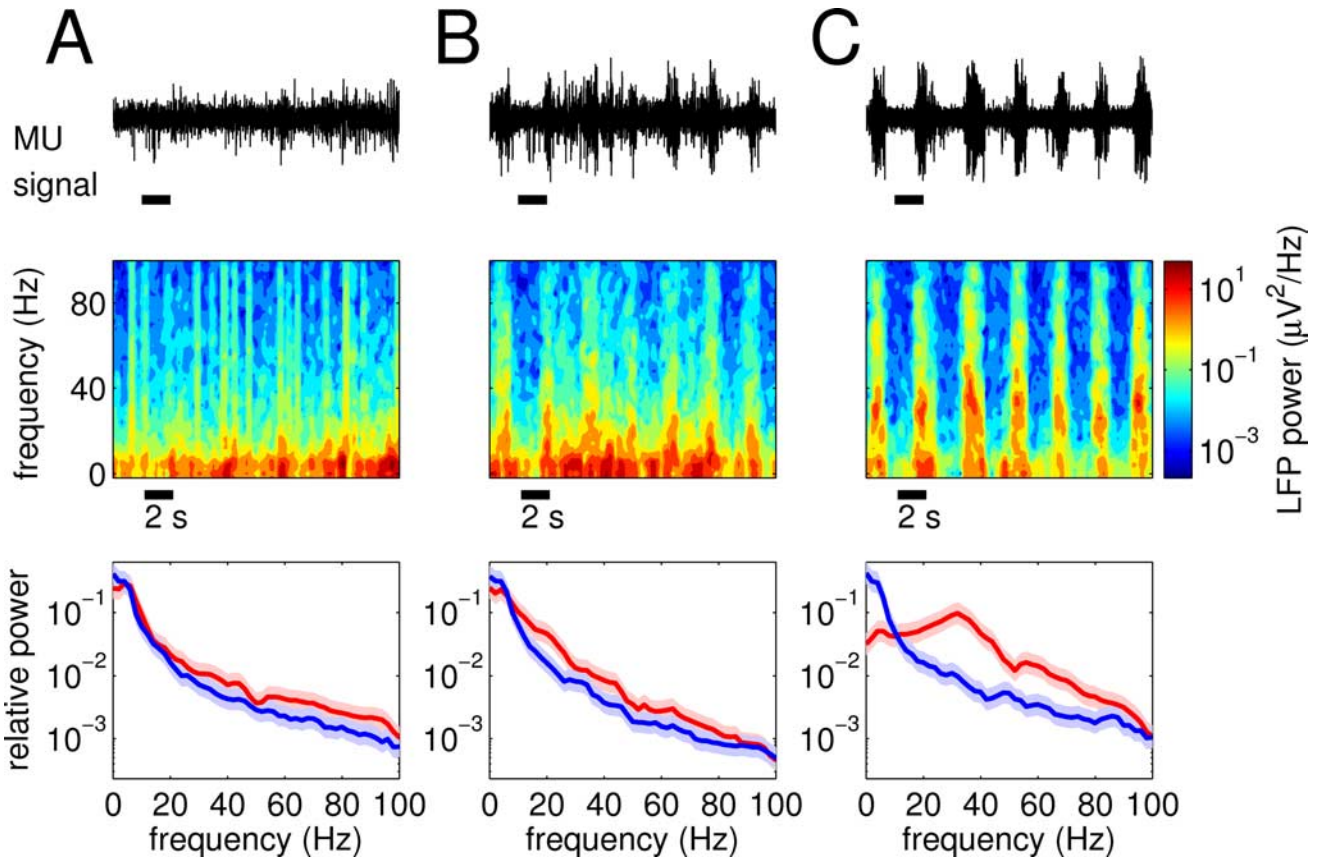

Figure 2. Fast oscillatory activity in the local network emerges only when the slow oscillations are fully developed. Spectrogram analysis of LFP recordings in a slice (as in Fig. 1), at different time points (9, 15, and 25 min in ***A***, ***B***, ***C***, respectively) after the change of extracellular bathing solution. Although the characteristic up states and down states were not observable in the MU signal of ***A*** and ***B*** (top panels), the same automated up state-down state detection protocol was applied to extract periods of higher and lower variance in the extracellular recording. The power spectrum analysis for these periods of differential variance is plotted in bottom panels (red = high variance periods, or up states; blue = low variance period, or down states. Shades indicate 95% CIs.). Different spectral signatures of high and low-variance field recordings appear only when the slow oscillation is fully developed (***C***), and not for periods of increasing but disorganized firing (***A***, ***B***).

(20–100 Hz). In a few slices ($n = 5$, 4 in visual and 1 in prefrontal cortex, see supplemental Fig. 1, available at www.jneurosci.org as supplemental material) we also identified a power peak at higher γ frequencies (~60 Hz).

Development of the fast oscillations

We tested whether fast oscillatory activity emerged during periods of enhanced disorganized firing, without the network having fully settled in the slowly oscillatory rhythmic repeating pattern. We recorded extracellularly from slices from the time when we changed the bathing solution until the slow oscillatory pattern was firmly established. As reported previously (Sanchez-Vives and McCormick, 2000), in this process neurons in the network start showing enhanced excitability early on, but only after a period (typically 15–30 min) these spontaneous activations organize in the slowly oscillatory network rhythm. Thus, this experiment allowed us to assess (1) whether the emergence of rapid oscillatory activity in the network was due to the change in external solution; and (2) whether rapid oscillatory activity was generally linked to enhanced network activation, or more specifically to the network activation that supports the slow oscillation. We used the methods described in Figure 1 to analyze pieces of LFP data at various time points through the development of this organized network activity. Our data showed that the spectral distinction in the β/γ range between periods of higher and lower network activations was only significant in the later phases of slow-oscillation development (see example in Fig. 2). This occurred in 4 of 4 slices recorded through the slow oscillation development. This finding indicates that these fast network oscillations emerge only when the network engages in the up state of rhythmic slow-oscillatory activity, and cannot result from general, unorganized network firing or simple ionic modifications.

Dynamics of multiunit spiking events

We wondered whether these fast oscillations were also reflected in the multiunit spiking activity (MUA) obtained from the extracellular recording (see Materials and Methods). We found that in some cases, MUA during up states did show clear marks of the oscillatory dynamics measured in the LFP (Fig. 3*A*,*B* shows the analysis for MUA data in the same recording for which LFP data are shown in Fig. 1). However, when taking together a population of measurements, the LFP analysis was more sensitive than the analysis of MUA data for the detection of fast oscillations in the up states. To compare with the data in the rest of our study, we show this in Figure 3*C* for a subpopulation of recordings ($n = 10$) for which intracellular data were simultaneous collected (see below). Although the power spectrum of LFP during the up state was significantly higher at 10–25 Hz than during down states (Fig. 3*C*, left), this was reflected in a barely significant structure in the MUA power spectrum at these frequencies (Fig. 3*C*, middle) and the MUA autocorrelation did not show any significant structure in these time scales (50–100 ms) (Fig. 3*C*, right). This weaker

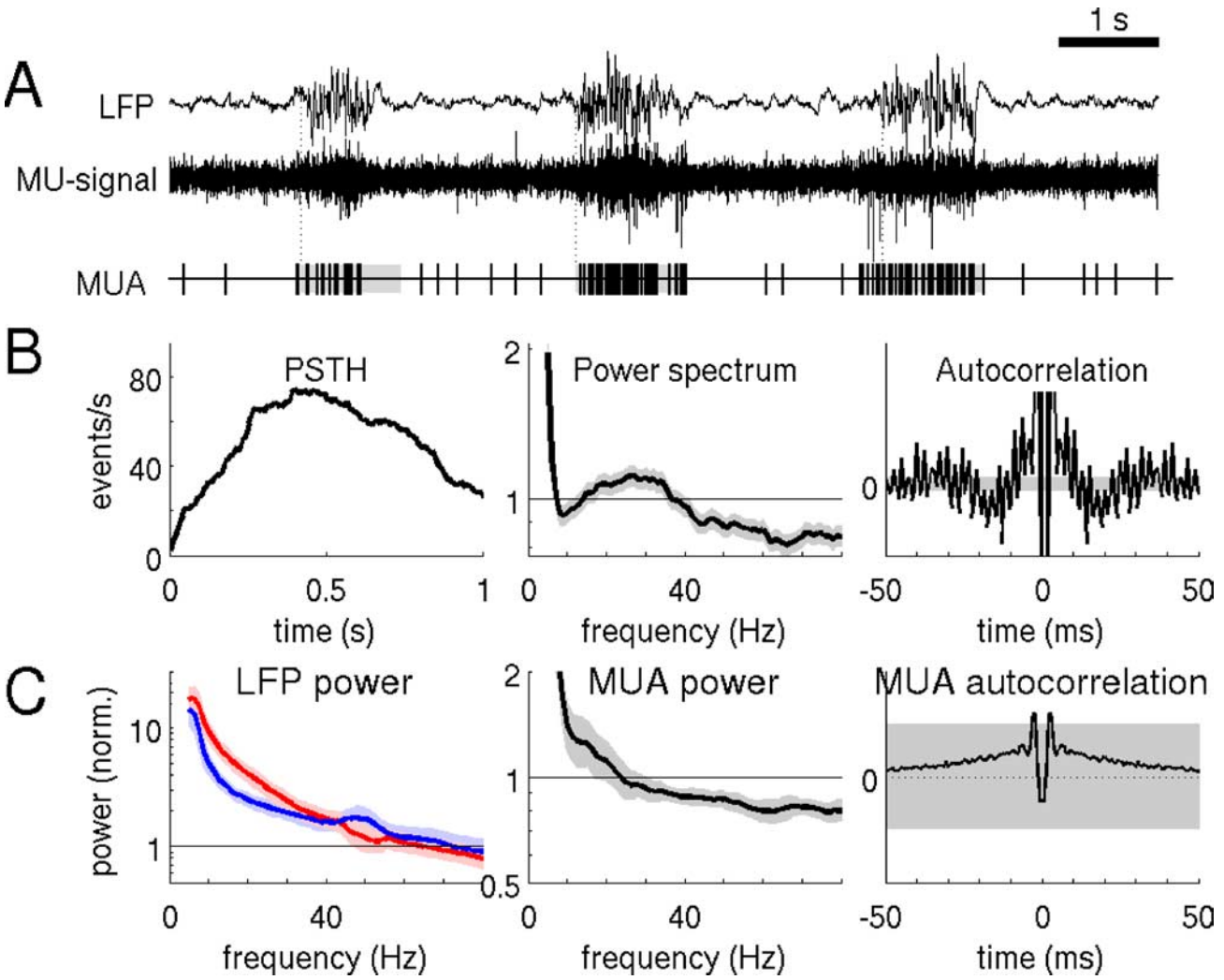

Figure 3. MUA can also reflect β/γ oscillations, but it is generally a less sensitive measure than LFP. ***A***, Example of the different data obtained from the extracellular recording: LFP signal (bandpass filtered, between 2 and 150 Hz), MU-extra (high-pass filtered, 5 Hz), and MUA (events thresholded from the high-pass filtered signal). ***B***, Analyses of the MUA data shown in ***A*** (same recording as shown in Fig. 1): time-histogram (PSTH, left) triggered by up state transitions detected from LFP (see Fig. 1); normalized power spectrum showing a peak in the β/γ range (middle); and autocorrelation function (right). ***C***, Average results for a population of 10 recordings (same as used in Figs. 4–10) show that although up states (red) had greater power in the β/γ band than down states (blue) as assessed from the LFP power spectra (left), this was not evidenced clearly in the averaged MUA power spectrum (middle) or in the averaged autocorrelation function (right). Shades indicate 95% CI.

synchrony in the MUA than in the LFP up states could be due to various reasons. On the one hand, neurons might be participating sparsely in the rhythm, so that each one of them fires only in a small subset of cycles of the population oscillation (Brunel and Wang, 2003). On the other hand, excitatory neurons might be overrepresented in the MUA, whereas interneurons are the ones that sustain the fast rhythms (Buhl et al., 1998; Fisahn et al., 1998; Penttonen et al., 1998; Traub et al., 2000; Whittington and Traub, 2003; Jonas et al., 2004; Hasenstaub et al., 2005; Mann and Paulsen, 2007). We studied this by looking at intracellular recordings taken in close proximity of the extracellular record.

No fast rhythms in the membrane voltage

Intracellular current clamp recordings were maintained at different membrane voltages by means of current injection. QX314 (100 μM) was added to the intracellular solution to block sodium channels and thus prevent the occurrence of action potentials when at depolarized potentials. At least three membrane voltages were usually attained: (1) approximately −70 mV, to achieve chloride reversal potential and isolate EPSPs, (2) ~0 mV, to isolate IPSPs, and (3) at a middle value, approximately −35 mV, to have a mixture of excitatory and inhibitory potentials. Taking a population of 10 such intracellular recordings (see below), we found that in one case we could identify a statistically significant difference in spectral content between up states and down states (Fig. 4*A*,*B*), but not in the average over the population of recordings ($n = 10$) (Fig. 4*C*). This result was consistent both for recordings at depolarized voltages and for recordings at hyperpolarized voltages. Thus, the fast fluctuations of membrane potential did not reflect the population rhythm detected extracellularly (compare Fig. 3*C*, left and Fig. 4*C* for the same dataset). We wondered whether extracting the timing of excitatory and inhibitory events from these records might provide a more sensitive measure of fast oscillatory activity or, alternatively, allow us to explore the differential involvement of excitation and inhibition.

Dynamics of synaptic events

The timing of presynaptic events of excitatory or inhibitory type were extracted from these intracellular recordings at different membrane voltages (Fig. 5). This was achieved by passing the

membrane voltage signal through a filter with response function $H(\omega)=i\omega$ (differentiator filter, see Materials and Methods), thus evaluating its first time derivative (Fig. 5*A*, top). Local maxima (minima) are then candidates for excitatory (inhibitory) events, as they represent the fastest voltage upward (downward) deflections in a neighborhood of data points. The values of these local extremes are typically Gaussian distributed with long tails (Fig. 5*D*). These long tails presumably contain actual synaptic events, which stick out from noisy membrane voltage fluctuations. To estimate the threshold value that separates these random voltage fluctuations from actual synaptic event voltage deflections, we detected events in the tails of the distribution beyond thresholds set at a fixed number n of interquartile ranges σ from the median of the distribution. The value of n was chosen independently for each recorded cell based on the requirement that as holding voltage was increased, either the number of detectable putative inhibitory events increased (because their driving force increased) or stayed constant (because input resistance decreased), or the number of putative excitatory events decreased (Fig. 5*E*). Ten of 14 neurons recorded at several holding voltages showed the required trend for at least one kind of events (excitatory or inhibitory) and were included in our subsequent analysis of synaptic event timings. We note here that synaptic events of equal polarity (either inhibitory or excitatory) extracted from membrane voltage recordings at different holding potentials had typically the same spectral signatures within a 95% confidence interval.

Isolated postsynaptic events (no other event in a window [−0 ms, 50 ms]) had an average amplitude of 2.58 ± 0.45 mV (range 0.44–5.23 mV) and a decay time constant of 27.9 ± 10.1 ms (range 6–111 ms) at a holding potential ~0 mV, and an amplitude of 1.17 ± 0.21 mV (range 0.41–2.67 mV) and a decay time constant of 28 ± 13 ms (range 3–127 ms) at a holding potential of approximately −70 mV. The amplitudes of putative excitatory postsynaptic potentials were thus significantly smaller than those of putative IPSPs (paired t test, $p=0.007$). Average event rates during up states were 36.6 ± 5.8 events/s and 26.7 ± 2.5 events/s for excitation and inhibition, respectively (mean ± SEM, paired t test $p = 0.19$, $n = 10$; ranges 10–73 and 15–43 events/s, respectively). This should be taken as an underestimation because our criteria for detecting events were strict (Fig. 5*A*,*C*, see subthreshold events), and because up states detected extracellularly were longer than those identified intracellularly (Fig. 6*A*,*B*). For down states excitatory events arrived at 3.2 ± 0.8 Hz and there were 5.9 ± 2.1 inhibitory events per second (mean ± SEM, paired t test $p = 0.21$, $n = 10$; ranges 0.2–7.2 and 0.1–23 events/s for excitation and inhibition, respec-

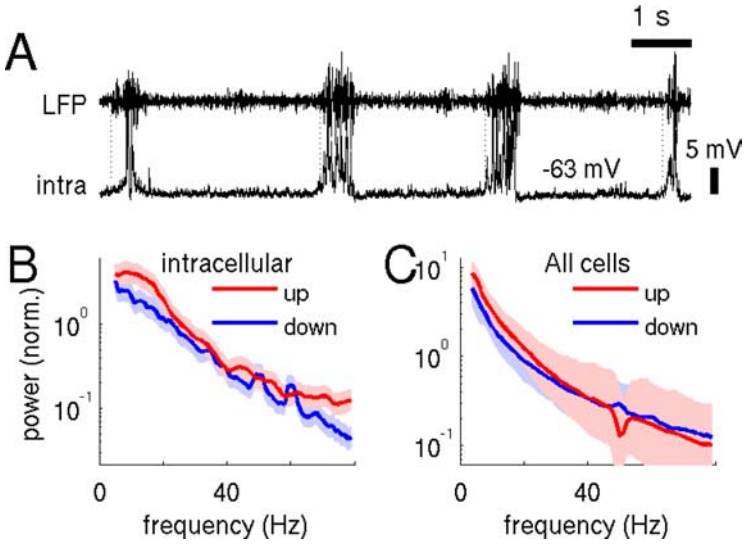

Figure 4. β/γ fluctuations in the neuronal membrane voltage were also less sensitive than LFPs. ***A***, Sample traces of simultaneously recorded LFP and neighboring intracellular membrane potential. ***B***, For this neuron, the power spectra of up states (red) and down states (blue) differed significantly in the β band. ***C***, In the population of 10 neurons analyzed, this difference was not significant. For the same population of recordings, LFP power spectra did differ significantly (Fig. 3*C*, left). Shades indicate 95% CI.

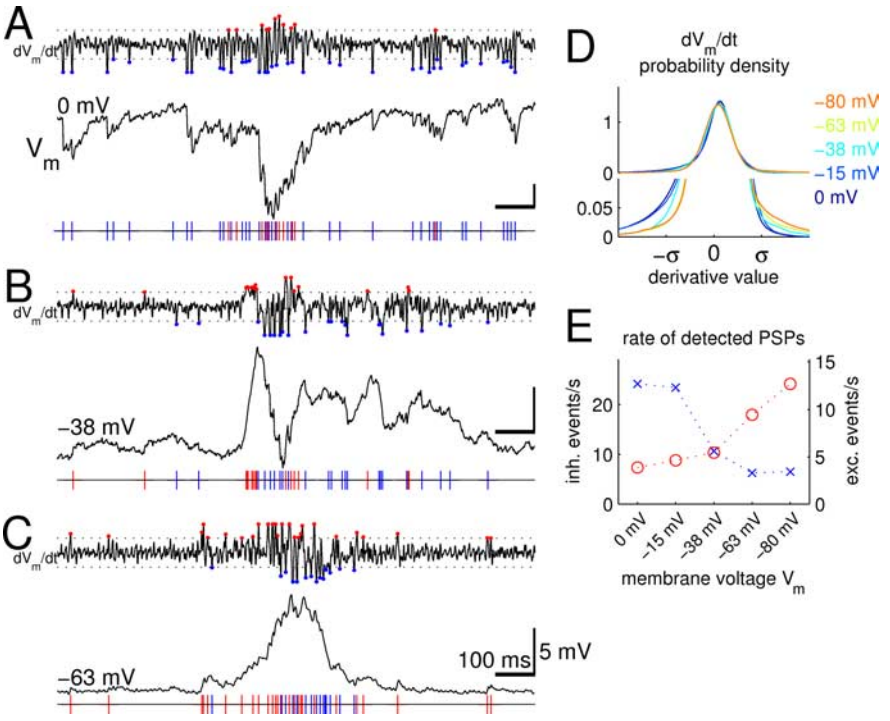

Figure 5. Detection of synaptic events from intracellular recordings at different membrane potential levels. ***A***, A differentiator filter was applied to the intracellular voltage signal V_m to obtain its derivative dV_m/dt (upper trace). dV_m/dt was thresholded (dotted lines, see also ***D***) both for positive (red dots) and negative (blue dots) local extremes. The timing of these events is attributed to the initiation of EPSPs or IPSPs, respectively, as represented in the event trains in the lower trace (red ticks = EPSPs, blue ticks = IPSPs). ***B–C***, Same as in ***A*** for a voltage trace obtained from the same neuron at different depolarization levels (QX314 in the electrode). Labeling on scale bars in ***C*** also applies to ***A–B***. ***D–E***, Method to select thresholds for dV_m/dt: histograms of dV_m/dt z-score values for different depolarization levels are plotted (***D***) and the threshold σ selected so that the amount of identified excitatory events (positive tail of histogram) decreases with depolarization, and the count of inhibitory events (negative tails) increases with depolarization (***E***). All data shown in this figure come from the same neuron.

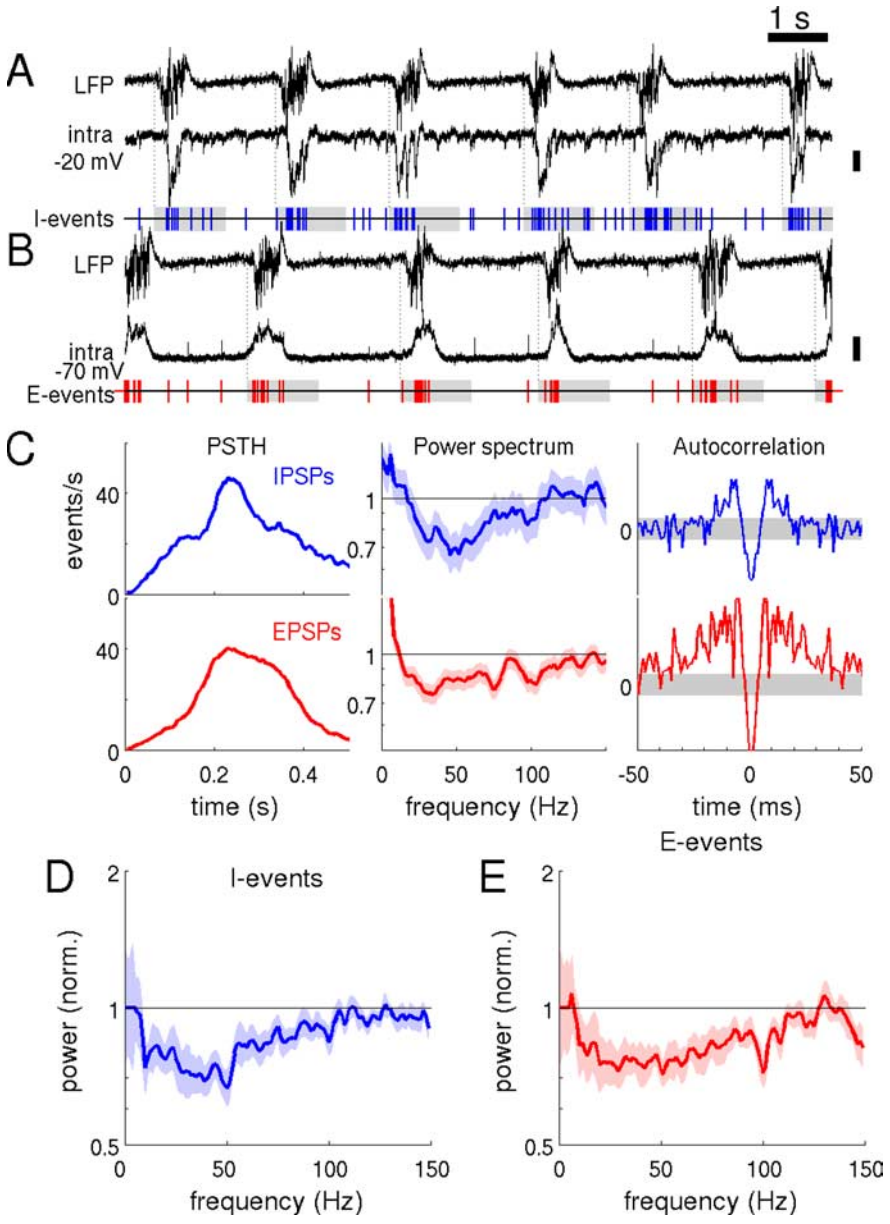

Figure 6. Example from a typical recording where synaptic events did not have a clear oscillatory character at β/γ frequencies. Inhibitory and excitatory events were identified from intracellular recordings at depolarized (−20 mV, ***A***) and hyperpolarized (−70 mV, ***B***) voltages, respectively, as explained in Figure 5. 1-s-long event-train fragments (grayed boxes on event spike trains in ***A***, ***B***) were aligned to up state onsets (dotted vertical lines in ***A***, ***B***) as identified from adjacent extracellular recordings (top traces in ***A***, ***B***). These fragments ($n = 59$ for ***A*** and $n = 187$ for ***B***) were collectively analyzed with an event histogram, power spectrum and autocorrelation function (***C***, see Materials and Methods). Data for inhibitory event trains is represented in blue and for excitatory event trains in red. Vertical scale bars on ***A*** and ***B*** correspond to 4 mV (intra). ***D***, Averaged power spectrum for inhibitory events in $n = 10$ recordings shows only a significant depression in power at low frequencies. ***E***, Same for excitatory events. Thus, in the population the temporal dynamics of synaptic event trains during the up states were primarily characterized by a short refractory period, and did not show significant oscillations. Shaded areas indicate 95% CIs for the corresponding estimation.

tively). Both excitatory and inhibitory events occurred at a significantly higher rate during up states than during down states (one-tailed paired t test $p < 0.001$, $n = 10$).

The temporal properties of the synaptic event trains detected in this way showed in a few cases (3 of 10) traces of rhythmic activity in the timing of inhibitory events, as revealed by power spectrum analysis (supplemental Fig. 2, available at www.jneurosci.org as supplemental material). In one case of 10, this was also observed for excitatory events (supplemental Fig. 3, available at www.jneurosci.org as supplemental material). However, the majority of event trains detected in our sample of neurons ($n = 10$) did not show oscillatory characteristics (Fig. 6*A–C*, typical neuron), and when we averaged power spectra for excitatory and inhibitory event trains through all our neuronal recordings ($n = 10$) the only consistent feature that emerged was a power depression <50 Hz (Fig. 6*D*,*E*). Although traces of 10–30 Hz oscillations were occasionally observed in individual event trains (supplemental Figs. 2, 3, available at www.jneurosci.org as supplemental material), these population characteristics indicate that event trains were mostly described by a Poisson point process with a short refractory period (Franklin and Bair, 1995; Compte et al., 2003b).

Neuronal events locked to network rhythm

We found an apparent inconsistency: LFP signals revealed robust oscillatory character in the β/γ bands, whereas events at the neuronal level, whether multiunit spikes detected extracellularly, neuronal membrane voltage, or synaptic events detected intracellularly, did not show consistent traces of oscillations in these frequency ranges. To evaluate whether such neuronal events had any consistent relation with the oscillation of the adjacent LFP, we computed the coherence between the intracellular recording and LFP signal, the spike-field coherence between the LFP and the MUA, and the event-field coherence between the LFP and the corresponding synaptic event train (see Materials and Methods). Figure 7 shows the results for one sample neuron (Fig. 7*A*,*B*,*D*,*F*, same neuron as in Fig. 4) and for the population of 10 recordings (Fig. 7*C*,*E*,*G*). We found significant coherence between the intracellular recording and the LFP (Fig. 7*B*, left), which manifested as a wiggled cross-correlation function (Fig. 7*B*, right). Indeed, when we averaged together coherence functions for each of 10 recorded neurons we found a very significant coherence value for frequencies <30 Hz, and most prominent ~20 Hz (Fig. 7*C*). Also, MUA spike trains typically showed a pronounced coherence with the LFP (Fig. 7*D*) and the population average showed a much more significant effect ~20 Hz (Fig. 7*E*) than the power spectrum analysis of Figure 3*C* (middle). Similarly, trains of synaptic events detected intracellularly in the neuron of Figure 7 had significant event-field coherence values with the LFP also at ~20 Hz (Fig. 7*F*, left), clearly seen also in the cross-correlation function (Fig. 7*F*, right). As we saw before, synaptic event trains in the population of recordings do not typically have a significant peak in the power spectrum (Fig. 6*D*,*E*). However, when we average together the event-field coherence for each of 10 sets of recordings we find a

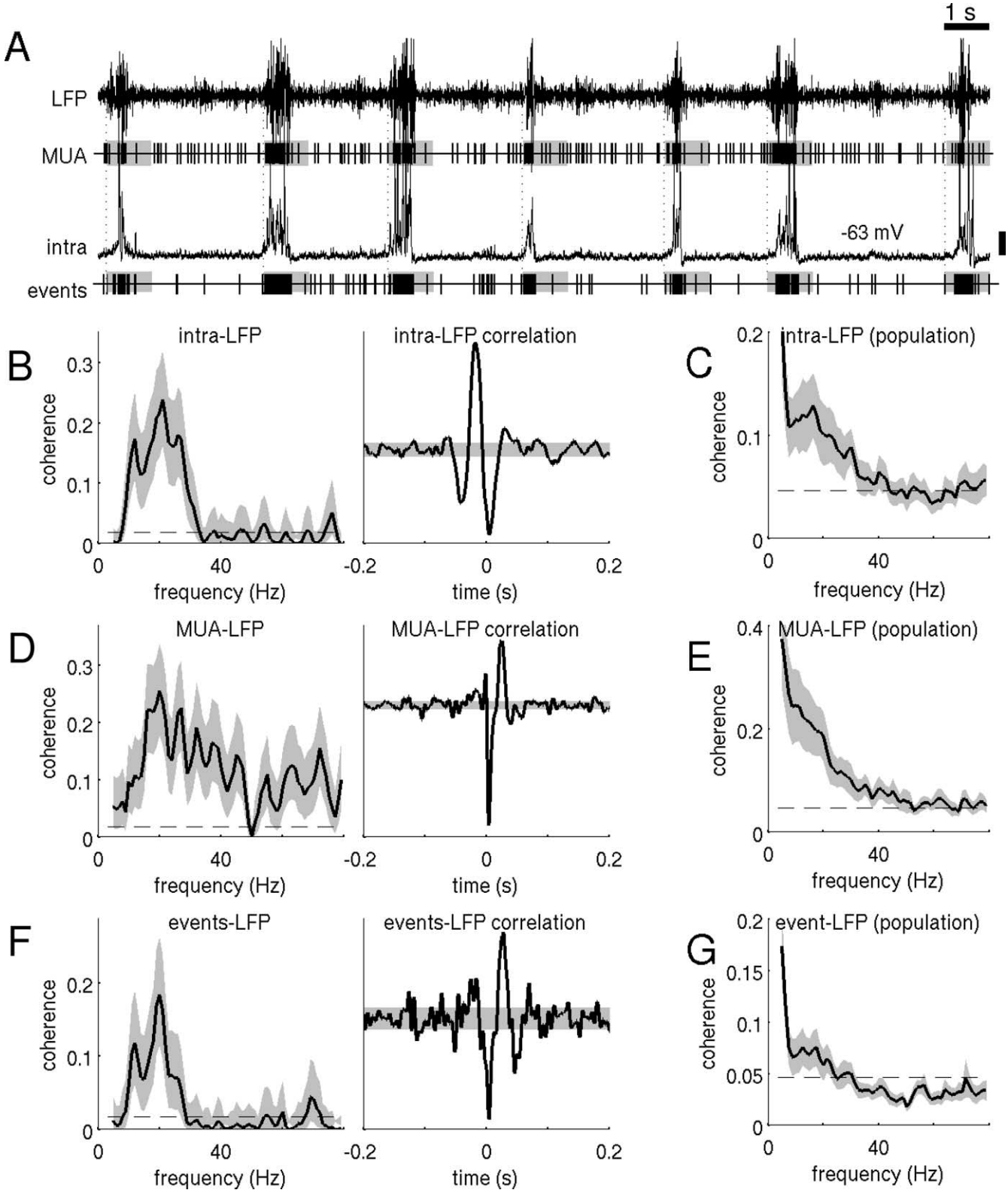

Figure 7. Intracellular, MUA, and synaptic event signals presented a robust β/γ coherence with the LFP, despite their weak oscillatory character (Figs. 3, 4, 6). ***A***, LFP, MUA, intracellular recordings, and extracted event train (see Fig. 5) for a 20 s window of activity for one neuron in our database, when recorded at a hyperpolarized membrane voltage (−63 mV). Vertical scale bar, 5 mV. ***B***, Coherence and cross-correlation function of this neuron's intracellular membrane voltage recording and the LFP. ***C***, In the population ($n = 10$), coherence between LFP and adjoining intracellular records was significant in the β/γ band. ***D***, Coherence and cross-correlation function between MUA and LFPs for the data shown in ***A***. ***E***, In the population ($n = 10$), coherence between MUA and LFP was significant in the β/γ band. ***F***, Coherence and cross-correlation function between event trains detected from the intracellular recording (Fig. 5) and simultaneous, adjoining LFP, for the neuron in ***A***. ***G***, Coherence between synaptic events and LFP remained significant in the population ($n = 10$). For this analysis, synaptic event trains recorded at different membrane voltages were analyzed conjointly (i.e., ignoring their putative excitatory or inhibitory character). In all panels, shading indicates the 95% CI of the estimate. Horizontal dashed lines mark the upper 95% CI under the hypothesis of independence.

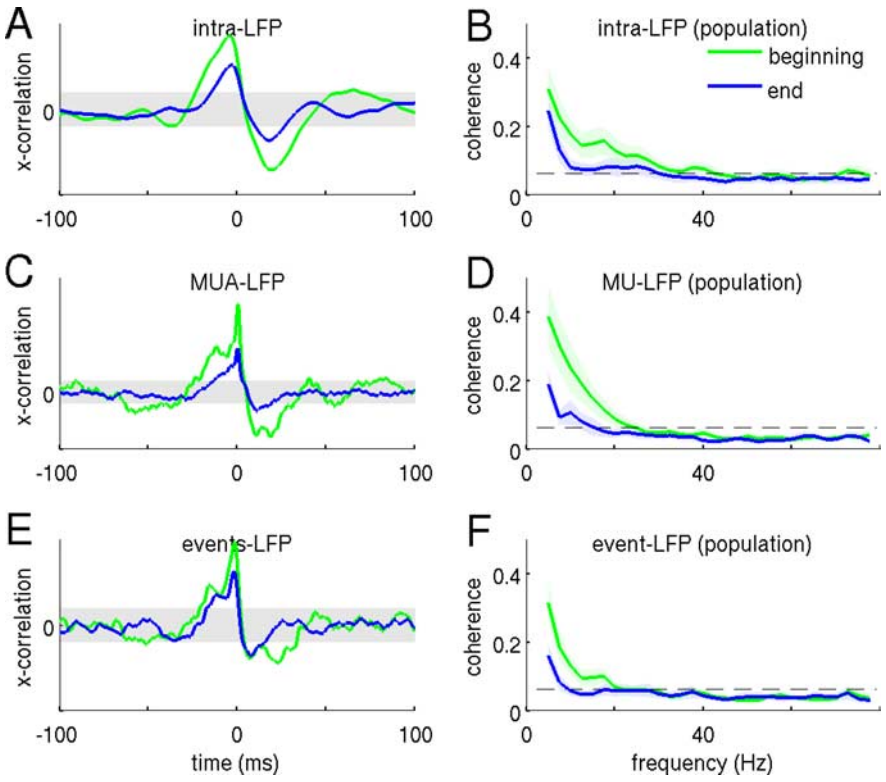

Figure 8. The β/γ rhythm is stronger at the beginning than at the end of the up state. Shorter windows of data, aligned either at the onset or at the offset of the up state to cover only the initial (green) or late (blue) phases of the up state, were used to compute the cross-correlation and coherence between the LFP and membrane voltage, MUA or event trains. Cross-correlations for a given neuron yielded stronger signals for the initial fragment of the up state (***A***, ***C***, ***E***). Also, the coherence averaged over the population ($n = 10$) retained significance mostly for data in the early up state (***B***, ***D***, ***F***). In all panels, shading indicates the 95% CI of the estimate. Dashed lines in ***B***, ***D***, and ***F*** mark the upper 95% CI under the hypothesis of independence.

significant coherence in the <20 Hz range (Fig. 7*G*). Thus, the lack of strong internal dynamics in MUA, membrane voltage and event trains in the β/γ range is reflecting a sparseness in how each neuron participates in the rhythm, so that the synchrony only becomes clear when one relates these small-sample measures with the global activity signal measured by the LFP.

Fast oscillations attenuate during the up state

Spiking and synaptic events did not relate equally to LFP activity at the beginning and at the end of the up state. To see this, we analyzed short (in each case, shorter than the duration of the up state) membrane voltage traces, MUA trains and event trains at the beginning and at the end of the up state. The corresponding cross-correlation functions for a typical neuron are shown in Figure 8*A*, *C*,*E*. We found systematically across our population ($n = 10$) that membrane voltage, MUA and synaptic events at the beginning of the up state had a significantly higher coherence with the LFP for frequencies <20 Hz than voltage or events at the end of the up state (Fig. 8). In addition, at the end of the up state, intracellular signals had lost their temporal relationship with the LFP in the β band, as they did not show a significant event-field coherence until frequencies below 10 Hz (Fig. 8*F*).

Inhibitory events carry the rhythm

We next explored the relationship between excitatory and inhibitory events, in relation to the extracellularly recorded rhythm. Figure 9*A*,*B* shows results for one neuron in our sample. Figure 9*A* shows that the membrane potential recorded at a depolarized membrane voltage (approximately −20 mV, sculpted primarily by inhibition) had a stronger cross-correlation function with the LFP than at more hyperpolarized voltage (approximately −80 mV, shaped mostly by excitation). Cross-correlation functions between synaptic events and LFP showed a consistent result: inhibitory events generated a much more significant cross-correlation than excitatory events (Fig. 9*B*). This was not specific of this sample neuron: when we evaluated separately intracellular recordings at depolarized and at hyperpolarized voltages, we found that membrane potential at depolarized voltages had a stronger coherence with the LFP across our population, especially significant at 20 Hz (Fig. 9*C*). Also the event-field coherence between events and LFP gave a significantly stronger coherence for inhibitory events than for excitatory events, with excitatory events not reaching a significant event-field coherence above 10 Hz (Fig. 9*D*).

Temporal relationship between inhibition and excitation

Apart from the relative strength of excitation and inhibition-mediated rhythms, our data might also provide information regarding the temporal relationship between excitation and inhibition within this network rhythm. We thus analyzed it carefully from various viewpoints. On the one hand, we resorted to the event trains detected at intermediate holding voltages (approximately −35 mV), between the reversal potentials of glutamate receptor channels and $GABA_A$ receptor channels. At these holding voltages, both EPSPs and IPSPs should be detectable through our method (Fig. 5). So, we had simultaneously recorded trains of excitatory and inhibitory events (sample in Fig. 10*A*, left, at −40 mV) from which to extract a coherence measure. For the sample neuron in Figure 10, excitatory and inhibitory events were strongly coherent at ~30 Hz (Fig. 10*A*, middle) and their cross-correlation function showed an out-of-phase relationship (Fig. 10*A*, right). We then assessed how robust these two observations were at the population level. First, we averaged together the coherence between excitatory and inhibitory events recorded at intermediate voltages in each of our neurons. The result showed significant coherence values in the range <30 Hz (Fig. 10*B*, left), indicating that excitatory and inhibitory events detected at intermediate voltages had a specific temporal relationship with each other. Second, we averaged together the coherency (see Materials and Methods) between excitatory and inhibitory events detected at intermediate voltages. The coherency is a complex-valued quantity (i.e., it is defined by two real numbers, an amplitude and a phase) whose squared amplitude is the coherence and whose phase is related to temporal shifts in the cross-correlation function. When averaging the coherency we take into account the phase of the relationship between the signals at each frequency. Thus, if we average together two signals with strong coherence but opposite phase their average coherence is big but their average coherency is small. The average coherency between excitation and inhibition in our database gave us a much suppressed coherency value, well below the 95% significance threshold for frequencies >10 Hz (Fig. 10*B*,

right). This showed that, although excitation and inhibition detected at intermediate voltages had a temporal relationship with each other, the phase was not consistent across the 10 sets of recordings.

cccEvents detected at the intermediate voltage are less robust than those detected at more extreme voltages, and this could explain the failure of the method to resolve a significant effect. We thus devised an alternative way to analyze the issue of the phase relationship between excitation and inhibition using only events detected at highly depolarized and hyperpolarized voltages. We did this by taking the event-field coherency for the inhibitory event train detected at depolarized voltages and the event-field coherency for the excitatory train detected at hyperpolarized voltages, and multiplying one by the complex-conjugate of the other (this mathematical operation reverses the phase of a complex number). The amplitude of this complex-valued quantity (which we will call event-field-event coherency) is large for those frequencies where both the excitatory and inhibitory trains present some event-field coherence, and its phase indicates the difference in phase between the inhibitory-field and excitatory-field relationships. We are thus relating nonsimultaneously recorded event trains through their comparison with the LFP, which remains unaffected in the stereotypically oscillating slice as one modifies the conditions of the intracellular recording. The results of this analysis showed that, across the selected set of intracellular recordings ($n = 10$), the average of the magnitude of this event-field-event coherence was significant for frequencies <30 Hz (Fig. 10*C*, left), whereas the magnitude of the average of event-field-event coherencies was nonsignificant for frequencies >10 Hz (Fig. 10*C*, right). These two results parallel the ones in Figure 10*B*, but extracted from entirely different event trains, so we conclude that our database does not support a stereotyped phase relationship between excitatory and inhibitory β/γ rhythmic firing in the cortical network during self-sustained spontaneous activity. We cannot discard, however, that resolving such phase relationship in a sparse cortical rhythm as this one (where synaptic events do not show an appreciable rhythm, Fig. 6, while being coherent with the network oscillation, Fig. 7) would require of a significantly larger database to reach statistical significance.

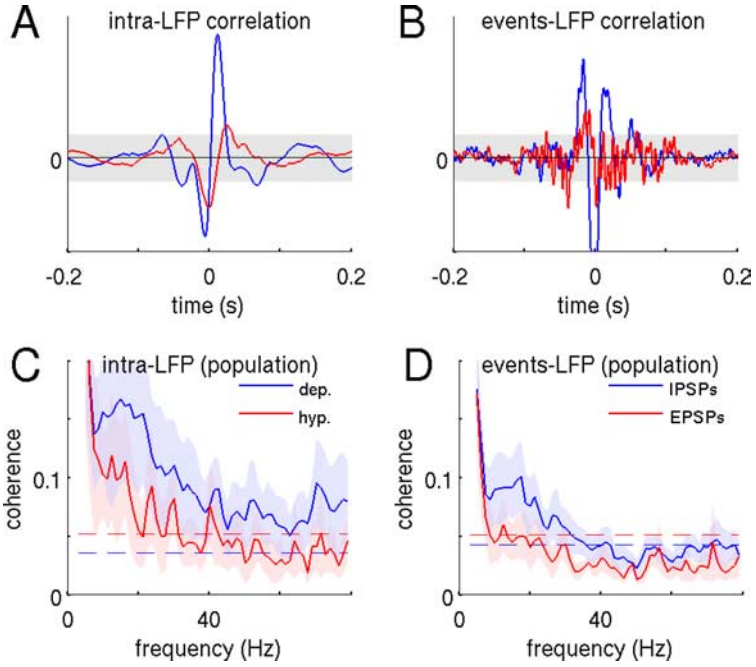

Figure 9. Inhibitory events are more coherent with the LFP than excitatory events. ***A***, Cross-correlation function between intracellular recording (blue = at −20 mV, red = at −80 mV) and LFP for a given neuron. ***B***, In the same recordings as in panel A, excitatory and inhibitory events were extracted from the intracellular recordings at different depolarization levels (see Fig. 5), and their coherence with the LFP was evaluated. The cross-correlation function (obtained from the coherence) is plotted here (blue = inhibitory events, red = excitatory events). ***C***, Coherence between intracellular recording (blue = at a depolarized level, red = at a hyperpolarized level) and LFP averaged over our sets of recordings ($n = 10$). ***D***, Coherence between excitatory (red) and inhibitory (blue) event trains averaged over the population ($n = 10$). Only inhibitory event coherence reaches significance in the β/γ range. In all panels, shading indicates the 95% CI of the estimate. Dashed lines in ***C*** and ***D*** mark the upper 95% CI under the hypothesis of independence.

Temporal dynamics during up states in a cortical network model

We have previously characterized slow oscillatory activity in cortical slices by means of an explicit biophysically detailed computational model of the cortical network (Compte et al., 2003a). This model consists of excitatory and inhibitory conductance-based neurons synaptically connected with a probability that decays with the distance between neurons (Fig. 11*A*). This is a realistic simplification of the architecture of the cortical microcircuit which can sustain activity closely mimicking the slow oscillatory activity recorded experimentally (Compte et al., 2003a) (Fig. 11*B*). We wondered whether this biophysically detailed model had the ingredients to reproduce also the fast oscillatory activity that we observed in the cortical slices. To this end we analyzed MUA collected from 60 neighboring pyramidal neurons centered at 8 different locations of the network in relation to the simulated LFP signal (this was the summated AMPA synaptic conductances on all neurons in the network), with exactly the same techniques as for Figure 10. Thus, the simulated LFP signal was analyzed to extract the envelope and from it the time of up state initiations (as described in Fig. 1*A*). These times were used to cut 1-s long pieces of the MUA data, and these pieces were analyzed with spectral methods for point processes and their spectra averaged together. We found that the autocorrelation and the power spectrum calculated in this way from the activity of the network reported in (Compte et al., 2003a) (note that there was not any parameter modification from the control network used in that manuscript) showed clear oscillatory activity ~10 Hz (Fig. 11*C*). This was observed only if spikes from sufficient neurons (at least 20) were pooled together in our synthetic MUA event trains. At the single cell level, oscillations went undetected in the averaged power spectrum of excitatory cells (supplemental Fig. 4, available at www.jneurosci.org as supplemental material). However, we noticed that oscillatory dynamics were more easily observed in the spike trains of model inhibitory interneurons, which showed an additional synchronization at 30–40 Hz (supplemental Fig. 4, available at www.jneurosci.org as supplemental material). Trains of spikes from neighboring inhibitory neurons also had slightly higher coherence with the model LFP signal than trains of spikes from excitatory neurons (supplemental Fig. 4, available at www.jneurosci.org as supplemental material), in agreement with our experimental results (Fig. 9). We then evaluated the temporal

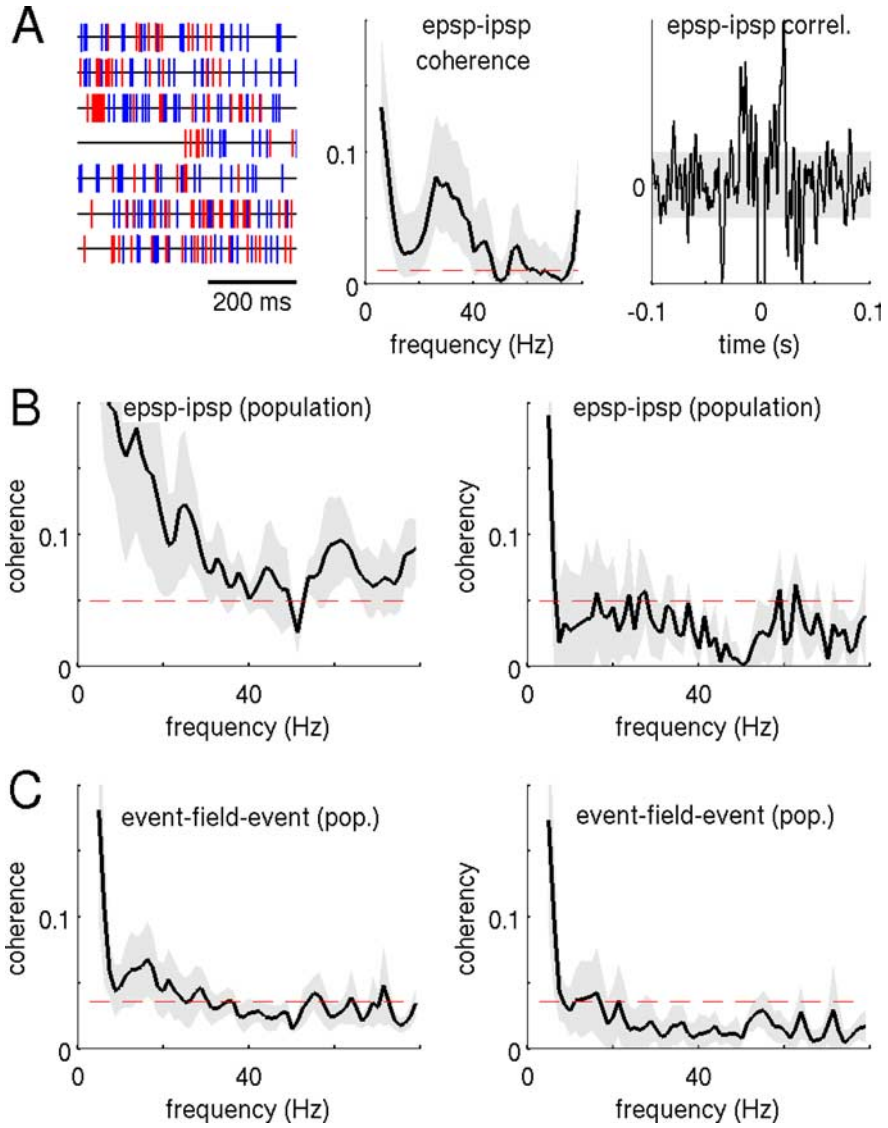

Figure 10. During the fast oscillations, inhibitory and excitatory events do not have a specific temporal relationship to each other. ***A***, Example analysis for an individual neuron in our database. Left, sample excitatory (red) and inhibitory (blue) event trains identified simultaneously from an intracellular recording at intermediate voltage depolarization (approximately −40 mV, see Fig. 5*B*). Middle, coherence between the excitatory and the inhibitory spike trains in ***A***. Right, cross-correlation function (obtained from the coherence in B) between excitatory and inhibitory events in ***A***. ***B***, Population results for the coherence (left) and for the coherency (right) between excitatory and inhibitory events averaged over the population ($n = 10$). Significant coherence and nonsignificant coherency in the β/γ band indicate the absence of a specific temporal relationship between excitation and inhibition during fast oscillations. ***C***, Parallel analysis using inhibitory trains extracted from depolarized records and excitatory trains extracted from hyperpolarized records, and constructing an event-field-event measure to evaluate if they have a consistent phase relationship to the LFP (see Materials and Methods). Event-field-event coherence (left) and coherency (right) parallel the result in ***B*** ($n = 10$). In all panels, shading indicates the 95% CI of the estimate. Red dashed lines mark the upper 95% CI under the hypothesis of independence.

relationship between excitatory and inhibitory spikes during the β rhythm by computing the coherency between their MUA trains. We found significant coherence at 10 Hz (coherence was 0.4 ± 0.09, mean ± 95% CI) with significantly positive phase (0.51 ± 0.21 radians, mean ± 95% CI). Thus, during the model network's β-range oscillation inhibitory neurons lagged excitatory neurons by 8.5 ± 3.6 ms (mean ± 95% CI).

Therefore, our cortical network model had the remarkable quality of mimicking simultaneously three apparently disconnected spontaneous behaviors of the isolated cortical network at disparate time and spatial scales: slow oscillatory activity in the 1–5 s range, fast oscillatory activity during up states in the 100 ms time scale, and activity propagation in the horizontal dimension covering the slice length in hundreds of milliseconds. This conjunction of observed behaviors reinforces the plausibility of the model presented in detail in (Compte et al., 2003a), and allows us to explore the mechanistic basis of high-frequency oscillations in the isolated cortical circuit. In particular, we investigated how the time constant τ_I of GABAergic synaptic conductances affects the fast oscillatory rhythm in our cortical network model. Simulations show that the primary frequency of these oscillations (evaluated as the peak of the power spectrum of multiunit spike trains sampled along the network, see above) is reduced as τ_I increases (Fig. 11*D*). This argues for the involvement of inhibitory synaptic transmission in the generation of this rhythm, as it has been suggested before (Buhl et al., 1998; Fisahn et al., 1998; Penttonen et al., 1998; Traub et al., 2000; Whittington and Traub, 2003; Jonas et al., 2004; Hasenstaub et al., 2005; Mann and Paulsen, 2007). However, in our computational model we can now investigate whether this role of inhibition is due to mutual inhibition between the inhibitory population or due to the inhibitory feedback between the excitatory and inhibitory populations. To this end, we modified parametrically the inhibitory conductances on either inhibitory (Fig. 11*E*) or excitatory (Fig. 11*F*) neurons in our model network, and we found that only the strength of inhibitory conductances to excitatory neurons had an effect on the frequency of the fast oscillations. We thus conclude that our network model supports the excitation-inhibition loop within the microcircuit as the primary mechanism for the generation of the fast oscillatory activity observed in the spontaneously active cortical slice *in vitro*. However, we also investigated other mechanisms present in our model neurons, and we found that also intrinsic properties of the excitatory cells on their own, such as the Ca^{2+}-dependent potassium current that is responsible for after-hyperpolarizations in these cells, have an impact in the properties of the fast oscillatory activity that is generated by the network (Fig. 11*G*). Thus, neuromodulatory manipulations that affect rather unspecifically both synaptic and intrinsic properties in the circuit will have effects on the network that are difficult to interpret in the computational model.

Experimental exploration of the mechanisms behind spontaneous fast oscillations *in vitro*

We tested the mechanistic predictions from the model in our experimental setup. We explored specifically two pharmacologi-

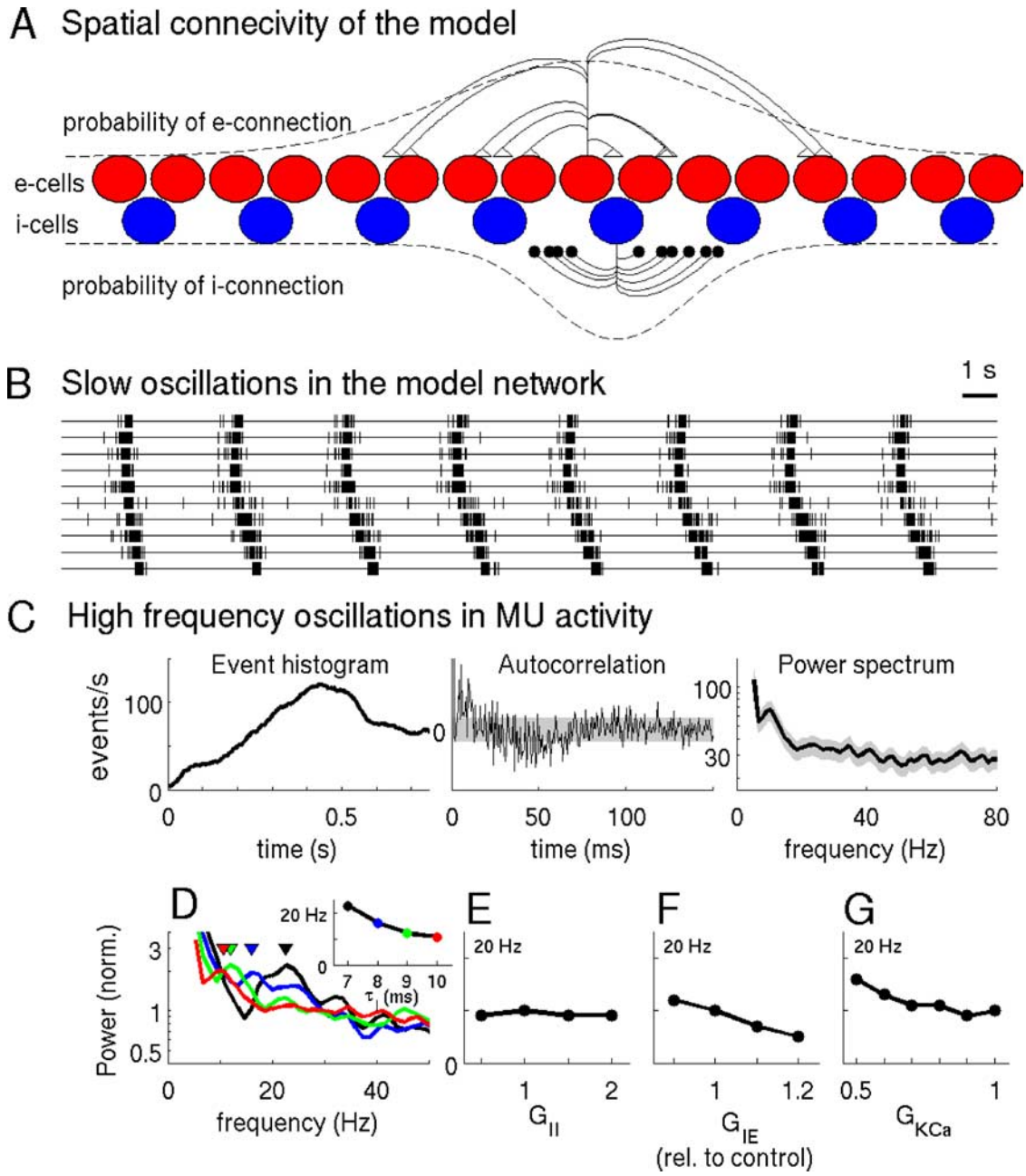

Figure 11. A computational network model of slow oscillatory activity also shows fast oscillations in the up states and allows for mechanistic explorations. ***A***, Schematic representation of the network architecture, with excitatory (red circles) and inhibitory (blue circles) neurons disposed on a line. Whether a neuron connected synaptically to another neuron at a given distance on the line was determined according to Gaussian probability densities (dashed curves). ***B***, Spontaneous activity in the network organizes in recurring bursts (frequency <1 Hz) that traveled along the network [see a complete description of this phenomenon in (Compte et al., 2003a)]. ***C***, Looking at the network activity during up states, fast oscillations could be detected from simulated multiunit records (event trains combining spikes from 60 neighboring neurons), both in the autocorrelation (middle panel) and in the power spectrum (right panel). Data from the computational model was analyzed with precisely the same methods and parameters as data from our *in vitro* experiments. ***D***, A parametric change in the decay time constant of inhibitory conductances τ_I ($\tau_I = 10, 9, 8, 7$ ms plotted in red, green, blue, and black, respectively. The control case in C corresponds to $\tau_I = 10$ ms), modified the power spectra of network activity parametrically, in that the frequency of the peak increased progressively as τ_I was reduced (see inset). ***E***, No change in the frequency of fast oscillations was detected when the inhibitory conductance between inhibitory neurons was modulated (from one half to double the control value). ***F***, Manipulation of the inhibitory conductance strength between inhibitory and excitatory neurons produced a parametric change in the frequency of the fast oscillation during the up states. ***G***, Manipulation of the conductance of a Ca^{2+}-dependent K^+ channel in excitatory neurons also had an effect in the frequency of the fast oscillation. Shades indicate 95% CI.

cal manipulations that have been used to study or induce fast oscillatory activity in *in vitro* preparations. On the one hand, we applied thiopental, which as a barbiturate is known to prolong the opening time of $GABA_A$ receptors (Lukatch and MacIver, 1996; Whittington et al., 1996). We analyzed the effects on fast oscillatory activity in our spontaneously active cortical slices of different dose applications, both using local and bath applications (see Materials and Methods). Locally applied thiopental (200 μM) had a consistent effect of eliminating the fast oscillatory activity, and greatly reducing the slow oscillation at the recorded site ($n = 9/12$). Bath application of thiopental (5–20 μM) had a dose-dependent effect, reducing markedly the frequency of fast oscillations (by as much as ~50%) while overall network activity concomitantly diminished ($n = 3$) (Fig. 12*A*,*B*). This result is in agreement with the computational model data shown before. This agreement with the model emphasizes the likelihood of an excitation-inhibition loop as the

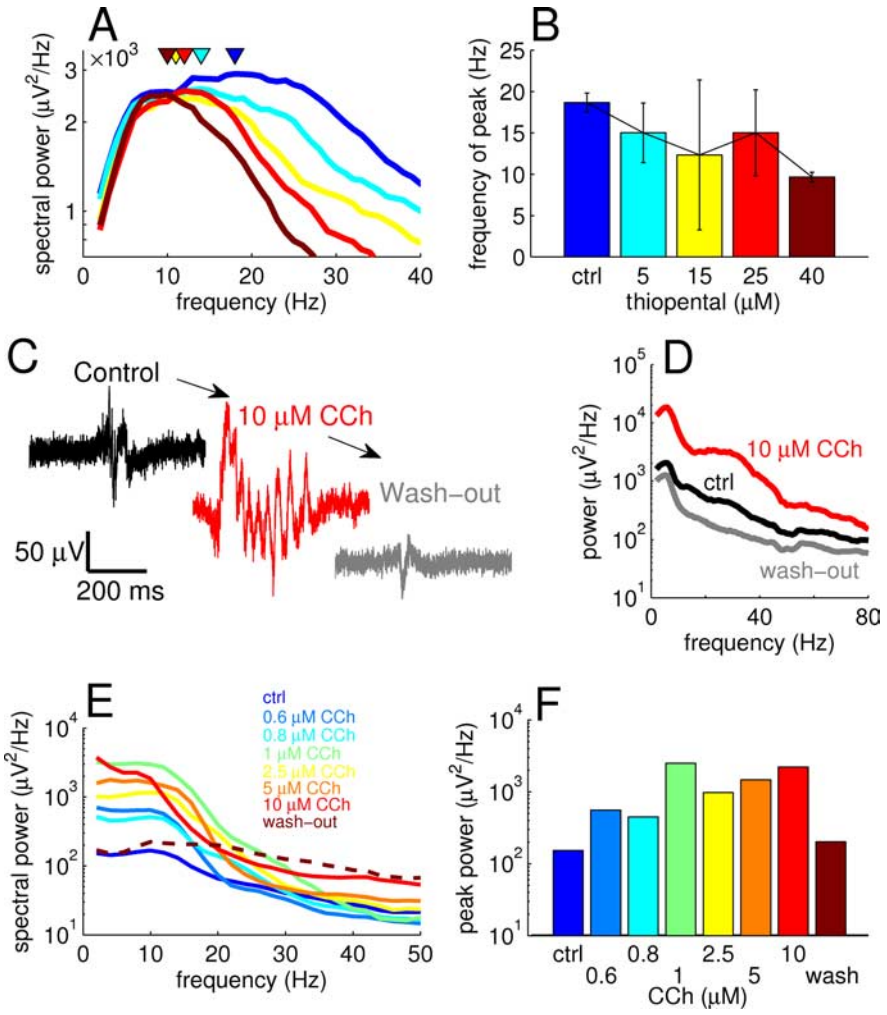

Figure 12. Pharmacological modulation of fast oscillatory activity during the up states of the slow oscillation. ***A***, Bath application of thiopental resulted in a dose-dependent modulation of the primary frequency of fast oscillations during up states. Power spectra (peaks indicated by inverted triangles) of LFPs during this pharmacological manipulation (colors indicate thiopental concentration as labeled in ***B***). ***B***, Frequency of power spectrum peak for $n = 3$ dose–response experiments, showing the same trend as the single experiment in ***A***. Error bars indicate SD. ***C***, Sample up states from LFPs in an experiment with bath application of CCh. ***D***, Power spectra of the recordings from which data in ***C*** were extracted show a reversible enhancement of β/γ oscillations by CCh. ***E–F***, Dose-dependence enhancement of β/γ activity by CCh.

basis of fast-frequency oscillation generation during slow oscillations in the cortical microcircuit. However, the strong reduction in frequency induced by thiopental could also be signaling a role for interneuronal networks (see Discussion).

In another set of experiments, we applied CCh, an acetylcholine receptor agonist. Local applications of CCh (20–100 μM) typically suppressed fast frequency oscillations ($n = 13/15$), and in one case enhanced them ($n = 1/15$). Bath application of CCh (0.5–5 μM), instead, showed a reversible and powerful augmentation of fast-frequency oscillations in the spontaneously active cortical network ($n = 3/4$; see an example in Fig. 12*C*,*D*). This enhancement of fast rhythms was also shown to be parametrically dependent on the dose of applied CCh (Fig. 12*E*,*F*). Carbachol has multiple effects on synaptic and intrinsic properties of the microcircuit (McCormick, 1992). The differential effects between local and bath applications could be due to the size of the affected network, or to dose-dependent CCh effects either on synaptic and/or intrinsic properties (Misgeld et al., 1986; Madison et al., 1987; Bal et al., 1994; Tiesinga et al., 2001).

Discussion

We have shown that the cortical microcircuit *in vitro* generates β/γ oscillations in the absence of externally applied neuromodulators or synaptic agonists, or electrical stimulation protocols. β/γ synchronization appears restricted to the up states of the slow oscillation (Figs. 1, 2). This is clearly seen in the population activity recorded with LFPs, but it goes usually undetected in MUA spike trains (Fig. 3), membrane voltage (Fig. 4) or the timing of incoming synaptic events (Fig. 6). However, spiking and synaptic events are phase-locked to the LFP β/γ rhythm (Fig. 7), and this is especially prominent for inhibitory events and at the beginning of the up state (Figs. 8, 9). Also, excitatory and inhibitory events maintain a coherent phase relationship with each other during β/γ rhythms, but this phase is not consistent across our population and we therefore cannot determine whether inhibition lags excitation or vice versa (Fig. 10). Finally, we tested an available computer model of slow oscillatory activity (Compte et al., 2003a) and found that β-range oscillations also emerged during up states and their frequency was controlled by the decay time constant of inhibitory synaptic currents (Fig. 11). We validated this prediction experimentally by bath-applying thiopental to the slowly oscillating slice (Fig. 12). As we discuss in the following, our findings in the slowly oscillating slice (Sanchez-Vives and McCormick, 2000) agree in a number of significant aspects with β/γ activity recorded *in vivo* and also qualitatively with earlier *in vitro* studies.

Individual neurons participate sparsely in the population rhythm: trains of synaptic events do not typically show a clear rhythm, but their timing is significantly phase-locked to the population oscillation. Sparse neuronal participation in high frequency rhythms is the physiological situation *in vivo* (Csicsvari et al., 1998, 1999; Fries et al., 2001; Logothetis et al., 2001). *In vitro* studies have also shown a similar behavior in pharmacologically activated cortical slices (Buhl et al., 1998; Fisahn et al., 1998; Fellous and Sejnowski, 2000). Here, we find weak β/γ sparse neuronal firing superimposed on the slow oscillation characteristic of slow-wave sleep (Steriade et al., 1993, 1996), underscoring its similitude with the cortical network dynamics *in situ*.

Computational network models of γ-range synchronization with sparse neuronal participation have implicated the time scales and strengths of fast excitatory and inhibitory currents in the control of the oscillation frequency (Brunel and Wang, 2003). Our computational model of slow oscillations concurs with this study, showing that β-oscillation frequency was modulated by the decay time constant of fast inhibitory currents, and the strength of the feedback loop between excitatory and inhibitory neurons (Fig. 11). Dose-dependent pharmacological treatment

of the slice with a barbiturate, known to prolong the opening time of $GABA_A$Rs (Lukatch and MacIver, 1996), confirmed experimentally this model prediction, finding a very substantial effect on oscillation frequency (Fig. 12). Earlier experiments on pharmacologically activated hippocampal slices had also observed this dose-dependent effect of barbiturates (Whittington et al., 1996; Dickinson et al., 2003).

Another common feature with earlier *in vivo* and *in vitro* studies is the higher degree of synchronization of inhibitory relative to excitatory neurons (Fig. 9) at β/γ frequencies (Whittington et al., 1995; Fisahn et al., 1998; Whittington and Traub, 2003; Hasenstaub et al., 2005; Bartos et al., 2007; Mann and Paulsen, 2007). Several physiological properties of basket cells have been hypothesized to underlie their pivotal role in β/γ synchronization: perisomatic synaptic targets (Mann and Paulsen, 2007), electrical synapses (Galarreta and Hestrin, 1999; Gibson et al., 1999; Whittington and Traub, 2003), and mutual shunting inhibition (Bartos et al., 2007). Our computational model reproduces predominant interneuron synchronization (supplemental Fig. 4, available at www.jneurosci.org as supplemental material) without incorporating electrical synapses or shunting inhibition. However, it is conceivable that in networks with heterogeneous interneuron populations (Gupta et al., 2000; Markram et al., 2004), electrical synapses and shunting inhibition become additional necessary mechanisms to sustain β/γ synchronization.

Together, the network γ observed here is mechanistically similar to earlier pharmacologically activated *in vitro* models of γ oscillations: cholinergic and glutamatergic models. However, two facts hint at a stronger association with kainate-activated *in vitro* slices (glutamatergic model). On the one hand, a substantial activation of cholinergic receptors is unlikely to occur spontaneously in a slice, given that the cholinergic inputs have been sectioned. However, significant kainate receptor activation is very plausible, as oscillations are restricted to the up state, when neurons are subject to a barrage of glutamatergic and GABAergic inputs (as in Sanchez-Vives and McCormick, 2000).

Our cortical microcircuit model simulates spontaneous neural activity *in vitro* across a range of time scales. It replicates infrequent (<1 Hz) transitions between membrane potential up states and down states, and the fast propagation of activity along the network (Compte et al., 2003a). Here, we show that model neurons are in addition synchronized at β frequencies (~10 Hz) and the model reproduces the experimental properties of this rhythm discussed above: sparse neuronal firing, frequency controlled by inhibition time constant, and higher synchronization of interneurons. In addition, the network model can address issues that cannot be decided experimentally. The experimental analysis could not resolve the temporal relationship between excitation and inhibition (Fig. 10). In the model we find that inhibitory spikes lag those emitted by excitatory neurons by a small fraction of the β cycle. Also, experiments cannot address whether inhibition-to-interneurons or inhibition-to-pyramidals determines the oscillation frequency. In the model, we found that only the inhibition-to-pyramidal conductance modulated the oscillation frequency. Thus, the model predicts that the excitation-inhibition loop underlies the β/γ oscillation. However, our finding that thiopental changes importantly the frequency of the fast oscillation does not exclude that networks of inhibitory neurons also participate. Indeed, several studies suggest that barbiturates have stronger effects when the rhythm is generated by an interneuron network than through a pyramidal-interneuron circuit (Whittington et al., 2000).

However, some aspects of model function are in disagreement with network activity measured experimentally. For instance, we found oscillatory traces (power spectrum peaks) in the spike trains of single inhibitory model neurons (supplemental Fig. 4, available at www.jneurosci.org as supplemental material), whereas inhibitory events did not typically show β/γ spectral peaks experimentally (Fig. 6, but see supplemental Figs. 2, 3, available at www.jneurosci.org as supplemental material). This discrepancy could reflect either frequent misses of our synaptic event detection protocol (Fig. 5) (see Materials and Methods), or the absence in our model of physiological mechanisms that determine the variability of neuronal activity in neocortical networks. One aspect that was not modeled was the unreliability of synaptic transmission. Overall, only 10% to 50% of spikes emitted by cortical interneurons result in a synaptic response postsynaptically (Gupta et al., 2000; Silberberg and Markram, 2007). This synaptic unreliability is even more accentuated for intracortical excitatory synaptic transmission (Markram et al., 1997, 1998; Silberberg and Markram, 2007). This mechanism would degrade the regularity of β/γ-range oscillations in synaptic events to model neurons, thus approaching the experimental results.

Previously studied *in vitro* preparations could generate γ synchronized activity through the pharmacological or electrical stimulation of cortical circuits (Traub et al., 2004). Very fast oscillations (>70 Hz) could emerge spontaneously in hippocampal slices (Draguhn et al., 1998), γ oscillations could be briefly induced with a puff of high-K^+ solution (LeBeau et al., 2002), but previous studies failed to detect robust γ-range oscillations in spontaneously active cortical slices (Hasenstaub et al., 2005). This raised the possibility that pharmacological manipulations were necessary to assemble the mechanisms of γ-range synchronization in cortical circuits (Börgers et al., 2005). Here, we show that the generation of β/γ oscillations in the local cortical circuit does not require exogenous electrical or pharmacological stimulation. Still, the mechanisms behind β/γ oscillations in our preparation do not differ appreciably from previous preparations. Therefore, rather than relying on specific pharmacological modulations, β/γ activity generation might depend just on a general, collective network activation that orchestrates appropriately the mechanisms available in local cortical circuits. Cholinergic agonists potentiate this emerging network rhythm (Fig. 12), indicating that neuromodulators may underlie the attentional or cognitive enhancement effects seen in neurophysiological recordings in behaving animals (Steinmetz et al., 2000; Fries et al., 2001; Pesaran et al., 2002; Womelsdorf et al., 2006; Saalmann et al., 2007).

We present here an *in vitro* model of cortical network synchronization in the β/γ range, which shares mechanisms with activity reported *in vivo* (Steriade et al., 1996; Hasenstaub et al., 2005; Mukovski et al., 2007) or in pharmacologically activated *in vitro* preparations (Traub et al., 2004). Simultaneous to this fast frequency rhythm, the network engages in the slow oscillatory activity characteristic of slow-wave sleep. These two rhythms coexist with very similar properties in the anesthetized animal *in vivo* (Steriade et al., 1996; Hasenstaub et al., 2005; Mukovski et al., 2007). This *in vitro* preparation, therefore, provides an approximate reproduction of the cortical network dynamics that characterize a well defined physiological state: slow-wave sleep. Slow oscillations during this brain state may be important for memory consolidation (Marshall et al., 2006; Marshall and Born, 2007), and ongoing fast oscillations might be involved in engaging spike timing-dependent synaptic plasticity to stabilize memories (Lengyel et al., 2005; Sejnowski and Paulsen, 2006). Further research using this *in vitro* preparation and its biophysically grounded computational model will help determine how net-

work dynamics at various time scales and the repertoire of plasticity mechanisms in the cortex interact in the course of slow-wave activity to stabilize network function, and how this may contribute to memory consolidation in the brain.

References

Aghajanian GK, Rasmussen K (1989) Intracellular studies in the facial nucleus illustrating a simple new method for obtaining viable motoneurons in adult rat brain slices. Synapse 3:331–338.

Bal T, Nagy F, Moulins M (1994) Muscarinic modulation of a pattern-generating network: control of neuronal properties. J Neurosci 14:3019–3035.

Bartos M, Vida I, Jonas P (2007) Synaptic mechanisms of synchronized gamma oscillations in inhibitory interneuron networks. Nat Rev Neurosci 8:45–56.

Bibbig A, Middleton S, Racca C, Gillies MJ, Garner H, Lebeau FE, Davies CH, Whittington MA (2007) Beta rhythms (15–20 Hz) generated by nonreciprocal communication in hippocampus. J Neurophysiol 97:2812–2823.

Börgers C, Epstein S, Kopell NJ (2005) Background gamma rhythmicity and attention in cortical local circuits: a computational study. Proc Natl Acad Sci U S A 102:7002–7007.

Brunel N, Wang XJ (2003) What determines the frequency of fast network oscillations with irregular neural discharges? I. Synaptic dynamics and excitation-inhibition balance. J Neurophysiol 90:415–430.

Buhl EH, Tamás G, Fisahn A (1998) Cholinergic activation and tonic excitation induce persistent gamma oscillations in mouse somatosensory cortex in vitro. J Physiol 513:117–126.

Compte A, Sanchez-Vives MV, McCormick DA, Wang XJ (2003a) Cellular and network mechanisms of slow oscillatory activity (<1 Hz) and wave propagations in a cortical network model. J Neurophysiol 89:2707–2725.

Compte A, Constantinidis C, Tegner J, Raghavachari S, Chafee MV, Goldman-Rakic PS, Wang XJ (2003b) Temporally irregular mnemonic persistent activity in prefrontal neurons of monkeys during a delayed response task. J Neurophysiol 90:3441–3454.

Crochet S, Chauvette S, Boucetta S, Timofeev I (2005) Modulation of synaptic transmission in neocortex by network activities. Eur J Neurosci 21:1030–1044.

Csicsvari J, Hirase H, Czurko A, Buzsáki G (1998) Reliability and state dependence of pyramidal cell-interneuron synapses in the hippocampus: an ensemble approach in the behaving rat. Neuron 21:179–189.

Csicsvari J, Hirase H, Czurkó A, Mamiya A, Buzsáki G (1999) Oscillatory coupling of hippocampal pyramidal cells and interneurons in the behaving Rat. J Neurosci 19:274–287.

Cunningham MO, Davies CH, Buhl EH, Kopell N, Whittington MA (2003) Gamma oscillations induced by kainate receptor activation in the entorhinal cortex in vitro. J Neurosci 23:9761–9769.

Dickinson R, Awaiz S, Whittington MA, Lieb WR, Franks NP (2003) The effects of general anaesthetics on carbachol-evoked gamma oscillations in the rat hippocampus in vitro. Neuropharmacology 44:864–872.

Draguhn A, Traub RD, Schmitz D, Jefferys JG (1998) Electrical coupling underlies high-frequency oscillations in the hippocampus in vitro. Nature 394:189–192.

Fellous JM, Sejnowski TJ (2000) Cholinergic induction of oscillations in the hippocampal slice in the slow (0.5–2 Hz), theta (5–12 Hz), and gamma (35–70 Hz) bands. Hippocampus 10:187–197.

Fisahn A, Pike FG, Buhl EH, Paulsen O (1998) Cholinergic induction of network oscillations at 40 Hz in the hippocampus in vitro. Nature 394:186–189.

Franklin J, Bair W (1995) The effect of a refractory period on the power spectrum of neuronal discharge. SIAM J Appl Math 55:1074–1093.

Fries P, Roelfsema PR, Engel AK, König P, Singer W (1997) Synchronization of oscillatory responses in visual cortex correlates with perception in interocular rivalry. Proc Natl Acad Sci U S A 94:12699–12704.

Fries P, Reynolds JH, Rorie AE, Desimone R (2001) Modulation of oscillatory neuronal synchronization by selective visual attention. Science 291:1560–1563.

Fries P, Schröder JH, Roelfsema PR, Singer W, Engel AK (2002) Oscillatory neuronal synchronization in primary visual cortex as a correlate of stimulus selection. J Neurosci 22:3739–3754.

Galarreta M, Hestrin S (1999) A network of fast-spiking cells in the neocortex connected by electrical synapses. Nature 402:72–75.

Gibson J, Beierlein M, Connors BW (1999) Two networks of electrically coupled inhibitory neurons in neocortex. Nature 402:75–79.

Gross J, Schnitzler A, Timmermann L, Ploner M (2007) Gamma oscillations in human primary somatosensory cortex reflect pain perception. PLoS Biol 5:e133.

Gupta A, Wang Y, Markram H (2000) Organizing principles for a diversity of GABAergic interneurons and synapses in the neocortex. Science 287:273–278.

Halliday DM, Rosenberg JR, Amjad AM, Breeze P, Conway BA, Farmer SF (1995) A framework for the analysis of mixed time series/point process data—theory and application to the study of physiological tremor, single motor unit discharges and electromyograms. Prog Biophys Mol Biol 64:237–278.

Hasenstaub A, Shu Y, Haider B, Kraushaar U, Duque A, McCormick DA (2005) Inhibitory postsynaptic potentials carry synchronized frequency information in active cortical networks. Neuron 47:423–435.

Jarvis MR, Mitra PP (2001) Sampling properties of the spectrum and coherency of sequences of action potentials. Neural Comput 13:717–749.

Jonas P, Bischofberger J, Fricker D, Miles R (2004) Interneuron Diversity series: Fast in, fast out–temporal and spatial signal processing in hippocampal interneurons. Trends Neurosci 27:30–40.

LeBeau FE, Towers SK, Traub RD, Whittington MA, Buhl EH (2002) Fast network oscillations induced by potassium transients in the rat hippocampus in vitro. J Physiol 542:167–179.

Lengyel M, Kwag J, Paulsen O, Dayan P (2005) Matching storage and recall: hippocampal spike timing-dependent plasticity and phase response curves. Nat Neurosci 8:1677–1683.

Logothetis NK, Pauls J, Augath M, Trinath T, Oeltermann A (2001) Neurophysiological investigation of the basis of the fMRI signal. Nature 412:150–157.

Lukatch HS, MacIver MB (1996) Synaptic mechanisms of thiopental-induced alterations in synchronized cortical activity. Anesthesiology 84:1425–1434.

Madison DV, Lancaster B, Nicoll RA (1987) Voltage clamp analysis of cholinergic action in the hippocampus. J Neurosci 7:733–741.

Mann EO, Paulsen O (2007) Role of GABAergic inhibition in hippocampal network oscillations. Trends Neurosci 30:343–349.

Markram H, Lübke J, Frotscher M, Roth A, Sakmann B (1997) Physiology and anatomy of synaptic connections between thick tufted pyramidal neurones in the developing rat neocortex. J Physiol 500:409–440.

Markram H, Wang Y, Tsodyks M (1998) Differential signaling via the same axon of neocortical pyramidal neurons. Proc Natl Acad Sci U S A 95:5323–5328.

Markram H, Toledo-Rodriguez M, Wang Y, Gupta A, Silberberg G, Wu C (2004) Interneurons of the neocortical inhibitory system. Nat Rev Neurosci 5:793–807.

Marshall L, Born J (2007) The contribution of sleep to hippocampus-dependent memory consolidation. Trends Cogn Sci 11:442–450.

Marshall L, Helgadóttir H, Mölle M, Born J (2006) Boosting slow oscillations during sleep potentiates memory. Nature 444:610–613.

McCormick DA (1992) Neurotransmitter actions in the thalamus and cerebral cortex and their role in neuromodulation of thalamocortical activity. Prog Neurobiol 39:337–388.

Melloni L, Molina C, Pena M, Torres D, Singer W, Rodriguez E (2007) Synchronization of neural activity across cortical areas correlates with conscious perception. J Neurosci 27:2858–2865.

Misgeld U, Calabresi P, Dodt HU (1986) Muscarinic modulation of calcium dependent plateau potentials in rat neostriatal neurons. Pflugers Arch 407:482–487.

Mitra PP, Pesaran B (1999) Analysis of dynamic brain imaging data. Biophys J 76:691–708.

Mukovski M, Chauvette S, Timofeev I, Volgushev M (2007) Detection of active and silent states in neocortical neurons from the field potential signal during slow-wave sleep. Cereb Cortex 17:400–414.

Penttonen M, Kamondi A, Acsády L, Buzsáki G (1998) Gamma frequency oscillation in the hippocampus of the rat: intracellular analysis in vivo. Eur J Neurosci 10:718–728.

Percival DB, Walden AT (1993) Spectral analysis for physical applications: multitaper and conventional univariate techniques. Cambridge: Cambridge UP.

Pesaran B, Pezaris JS, Sahani M, Mitra PP, Andersen RA (2002) Temporal

structure in neuronal activity during working memory in macaque parietal cortex. Nat Neurosci 5:805–811.
Reig R, Sanchez-Vives MV (2007) Synaptic transmission and plasticity in an active cortical network. PLoS ONE 2:e670.
Roopun AK, Middleton SJ, Cunningham MO, LeBeau FE, Bibbig A, Whittington MA, Traub RD (2006) A beta2-frequency (20–30 Hz) oscillation in nonsynaptic networks of somatosensory cortex. Proc Natl Acad Sci U S A 103:15646–15650.
Saalmann YB, Pigarev IN, Vidyasagar TR (2007) Neural mechanisms of visual attention: how top-down feedback highlights relevant locations. Science 316:1612–1615.
Sanchez-Vives MV, McCormick DA (2000) Cellular and network mechanisms of rhythmic recurrent activity in neocortex. Nat Neurosci 3:1027–1034.
Sejnowski TJ, Paulsen O (2006) Network oscillations: emerging computational principles. J Neurosci 26:1673–1676.
Silberberg G, Markram H (2007) Disynaptic inhibition between neocortical pyramidal cells mediated by Martinotti cells. Neuron 53:735–746.
Singer W, Gray CM (1995) Visual feature integration and the temporal correlation hypothesis. Annu Rev Neurosci 18:555–586.
Steinmetz PN, Roy A, Fitzgerald PJ, Hsiao SS, Johnson KO, Niebur E (2000) Attention modulates synchronized neuronal firing in primate somatosensory cortex. Nature 404:187–190.
Steriade M, Amzica F, Contreras D (1996) Synchronization of fast (30–40 Hz) spontaneous cortical rhythms during brain activation. J Neurosci 16:392–417.
Steriade M, Contreras D, Curró Dossi R, Nuñez A (1993) The slow (< 1 Hz) oscillation in reticular thalamic and thalamocortical neurons: scenario of sleep rhythm generation in interacting thalamic and neocortical networks. J Neurosci 13:3284–3299.
Tallon-Baudry C, Bertrand O, Peronnet F, Pernier J (1998) Induced gamma-band activity during the delay of a visual short-term memory task in humans. J Neurosci 18:4244–4254.
Tallon-Baudry C, Mandon S, Freiwald WA, Kreiter AK (2004) Oscillatory synchrony in the monkey temporal lobe correlates with performance in a visual short-term memory task. Cereb Cortex 14:713–720.
Thomson DJ, Chave AD (1991) Jackknifed error estimates for spectra, coherences, and transfer functions. In: Advances in spectrum analysis and array processing (Haykin S ed.), pp 58–113. Englewood Cliffs, NJ: Prentice-Hall.
Tiesinga PH, Fellous JM, José JV, Sejnowski TJ (2001) Computational model of carbachol-induced delta, theta, and gamma oscillations in the hippocampus. Hippocampus 11:251–274.
Traub R, Bibbig A, LeBeau F, Cunningham M, Whittington M (2005) Persistent gamma oscillations in superficial layers of rat auditory neocortex: experiment and model. J Physiol 562:3–8.
Traub RD, Bibbig A, Fisahn A, LeBeau FE, Whittington MA, Buhl EH (2000) A model of gamma-frequency network oscillations induced in the rat CA3 region by carbachol in vitro. Eur J Neurosci 12:4093–4106.
Traub RD, Bibbig A, LeBeau FE, Buhl EH, Whittington MA (2004) Cellular mechanisms of neuronal population oscillations in the hippocampus in vitro. Annu Rev Neurosci 27:247–278.
Volgushev M, Chauvette S, Mukovski M, Timofeev I (2006) Precise long-range synchronization of activity and silence in neocortical neurons during slow-wave oscillations [corrected]. J Neurosci 26:5665–5672.
Wang XJ (1999) Synaptic basis of cortical persistent activity: the importance of NMDA receptors to working memory. J Neurosci 19:9587–9603.
Wang XJ, Buzsáki G (1996) Gamma oscillation by synaptic inhibition in a hippocampal interneuronal network model. J Neurosci 16:6402–6413.
Whittington MA, Traub RD (2003) Interneuron diversity series: inhibitory interneurons and network oscillations in vitro. Trends Neurosci 26:676–682.
Whittington MA, Traub RD, Jefferys JG (1995) Synchronized oscillations in interneuron networks driven by metabotropic glutamate receptor activation. Nature 373:612–615.
Whittington MA, Jefferys JG, Traub RD (1996) Effects of intravenous anaesthetic agents on fast inhibitory oscillations in the rat hippocampus in vitro. Br J Pharmacol 118:1977–1986.
Whittington MA, Stanford IM, Colling SB, Jefferys JG, Traub RD (1997) Spatiotemporal patterns of gamma frequency oscillations tetanically induced in the rat hippocampal slice. J Physiol 502:591–607.
Whittington MA, Traub RD, Kopell N, Ermentrout B, Buhl EH (2000) Inhibition-based rhythms: experimental and mathematical observations on network dynamics. Int J Psychophysiol 38:315–336.
Womelsdorf T, Fries P, Mitra PP, Desimone R (2006) Gamma-band synchronization in visual cortex predicts speed of change detection. Nature 439:733–736.
Womelsdorf T, Schoffelen JM, Oostenveld R, Singer W, Desimone R, Engel AK, Fries P (2007) Modulation of neuronal interactions through neuronal synchronization. Science 316:1609–1612.